NATIONAL ADVISORY COMMITTEE FOR AERONAUTICS

TECHNICAL NOTE 3373

THEORETICAL CALCULATIONS OF THE PRESSURES, FORCES, AND MOMENTS DUE TO VARIOUS LATERAL MOTIONS ACTING ON THIN ISOLATED VERTICAL TAILS WITH SUPERSONIC LEADING AND TRAILING EDGES

By Kenneth Margolis

Langley Aeronautical Laboratory
Langley Field, Va.

Washington
March 1955

NATIONAL ADVISORY COMMITTEE FOR AERONAUTICS

TECHNICAL NOTE 3373

THEORETICAL CALCULATIONS OF THE PRESSURES, FORCES, AND MOMENTS DUE TO VARIOUS LATERAL MOTIONS ACTING ON THIN ISOLATED VERTICAL TAILS WITH SUPERSONIC LEADING AND TRAILING EDGES

By Kenneth Margolis

SUMMARY

Velocity potentials and pressure distributions due to various lateral motions are derived for a family of thin isolated vertical tails with arbitrary sweepback and taper ratio by applying linearized thin-airfoil theory for supersonic speeds. Motions considered in the analysis are steady rolling, steady yawing, and constant lateral acceleration. For the particular cases of triangular (half-delta) and rectangular vertical tails, integrated forces and moments expressed in the form of stability derivatives are also derived. All results are, in general, applicable at those supersonic speeds for which both the tail leading and trailing edges are supersonic. For purposes of completeness, analogous expressions and derivatives for sideslip motion obtained primarily from other sources are included.

Expressions for potentials, pressures, and stability derivatives are tabulated. Curves for the stability derivatives are presented which enable rapid estimation of their values for given values of aspect ratio and Mach number. In order to indicate the importance of end-plate effects, several comparisons are shown of the derived results (based on a zero-end-plate analysis) with those corresponding to a complete-end-plate analysis.

INTRODUCTION

Detailed knowledge of the loading, forces, and moments acting on vertical tails undergoing various maneuvers is a necessary prerequisite for determining the lateral dynamic behavior of aircraft traveling at supersonic speeds. The information presently available is, in many instances, insufficient to enable reliable estimates to be made of the

contribution of the vertical tail to airplane stability. Aside from calculations for several "slender" configurations (e.g., refs. 1 to 7), most of the theoretical efforts along these lines have been restricted primarily to sideslip motion (refs. 8 and 9). A recent paper (ref. 10) treats the calculation of pressures, forces, and moments due to several types of lateral motion acting on thin, isolated, triangular vertical tails. The range of speeds considered therein requires that the tail leading edge be subsonic and the tail trailing edge supersonic.

The present paper is also concerned with the calculation of pressures, forces, and moments acting on thin isolated vertical tails subject to various lateral motions. The speed range for the present investigation, however, is higher than that of reference 10; both the leading and trailing edges of the vertical tail must be supersonic. The vertical tail is of fairly general plan form having arbitrary sweepback, aspect ratio, and taper ratio (tip and root chords parallel). Four motions are treated: steady rolling, steady yawing, constant sideslip, and constant lateral acceleration.

The half-delta and rectangular vertical tails are analyzed in detail. Forces and moments (expressed in the form of stability derivatives) and their variations with Mach number and aspect ratio are presented in a series of simple charts. In order to gain some insight into the possible effects of an end plate, several of the derived results are compared with corresponding calculations based on a complete-end-plate analysis. (A complete-end-plate analysis implies that the horizontal tail acts as a perfect reflection plane.)

SYMBOLS

x,y,z	Cartesian coordinates used in analysis (see fig. 2(a))
V	free-stream or flight velocity (see fig. 2)
ρ	density of air
q	dynamic pressure, $\frac{1}{2}\rho V^2$
φ	perturbation velocity potential due to particular motion under consideration, evaluated on negative y-side of tail surface (see fig. 2)
$\Delta\varphi$	difference in perturbation velocity potential between two sides of tail surface, $\varphi(x,0^+,z) - \varphi(x,0^-,z)$

$\Delta P/q$	coefficient of pressure difference between two sides of tail surface due to particular motion under consideration, positive in sense of positive side force (see fig. 2)
M	Mach number, $\frac{V}{\text{Speed of sound}}$
$B = \sqrt{M^2 - 1}$	
b	span of vertical tail
c_r	root chord of vertical tail
λ	taper ratio, Tip chord/Root chord
m	slope of tail leading edge; cotangent of leading-edge sweepback angle (see fig. 1)
A	aspect ratio of vertical tail, b^2/S
S	area of vertical tail
β	angle of sideslip
p,r	angular velocities about x- and z-axes, respectively (see fig. 2)
t	time
$\dot{\beta}$	rate of change of β with time, $d\beta/dt$
Y	side force
N	yawing moment
L'	rolling moment
C_Y	side-force coefficient, Y/qS
C_n	yawing-moment coefficient, N/qSb
C_l	rolling-moment coefficient, L'/qSb
$C_{Y_\beta} = \left(\frac{\partial C_Y}{\partial \beta}\right)_{\beta \to 0}$	

$$C_{n_\beta} = \left(\frac{\partial C_n}{\partial \beta}\right)_{\beta \to 0}$$

$$C_{l_\beta} = \left(\frac{\partial C_l}{\partial \beta}\right)_{\beta \to 0}$$

$$C_{Y_p} = \left(\frac{\partial C_Y}{\partial \frac{pb}{V}}\right)_{p \to 0}$$

$$C_{n_p} = \left(\frac{\partial C_n}{\partial \frac{pb}{V}}\right)_{p \to 0}$$

$$C_{l_p} = \left(\frac{\partial C_l}{\partial \frac{pb}{V}}\right)_{p \to 0}$$

$$C_{Y_r} = \left(\frac{\partial C_Y}{\partial \frac{rb}{V}}\right)_{r \to 0}$$

$$C_{n_r} = \left(\frac{\partial C_n}{\partial \frac{rb}{V}}\right)_{r \to 0}$$

$$C_{l_r} = \left(\frac{\partial C_l}{\partial \frac{rb}{V}}\right)_{r \to 0}$$

$$C_{Y_{\dot{\beta}}} = \left(\frac{\partial C_Y}{\partial \frac{\dot{\beta} b}{V}}\right)_{\dot{\beta} \to 0}$$

$$C_{n_{\dot{\beta}}} = \left(\frac{\partial C_n}{\partial \frac{\dot{\beta} b}{V}}\right)_{\dot{\beta} \to 0}$$

$$C_{l_{\dot{\beta}}} = \left(\frac{\partial C_l}{\partial \frac{\dot{\beta} b}{V}}\right)_{\dot{\beta} \to 0}$$

Subscripts:

1,2	components used for $\dot{\beta}$-derivatives
β=1	due to unit sideslip condition
r=1	due to unit yawing condition

Abbreviations:

L.E.	leading edge
T.E.	trailing edge

All angles are measured in radians.

ANALYSIS

Scope

The general vertical-tail plan form considered herein is shown in figure 1(a). The leading edge has arbitrary sweepback and the trailing edge may be either sweptback or sweptforward; the root and tip chords are parallel to each other and the tail is tapered in the conventional sense. The permissible ranges of sweep, aspect ratio, and taper ratio for any given Mach number are determined by the conditions (indicated in fig. 1) that both the leading and trailing edges remain supersonic and that the Mach line emanating from the leading edge of the root chord does not intersect the tip chord.

Expressions based on linearized supersonic-flow theory are obtained for the perturbation velocity potentials and pressure distributions due to steady rolling, steady yawing, and constant lateral acceleration. For purposes of completeness, analogous results for constant sideslip motion obtainable, in general, from reference 8 are included. The expressions, which are derived for the condition of zero geometric angle of attack and which are valid for low rates of angular velocities, small sideslip angles, and small angle-of-sideslip variation with time, are tabulated so that they may be utilized conveniently in the calculation of load distributions and the corresponding forces and moments for the general sweptback tapered tail surface.

Two important members of the general vertical-tail family are considered in detail. These are the rectangular tail (shown in fig. 1(b)) and the triangular tail with an unswept trailing edge, that is, the half-delta tail (shown in fig. 1(c)). For these tails, closed-form expressions

are derived for the side force, yawing moment, and rolling moment due to each motion. The resulting formulas are expressed in the form of stability derivatives and are tabulated; simple charts are presented which permit rapid estimation of the 12 stability derivatives for given values of aspect ratio and Mach number.

Three systems of body axes are employed in the present paper. For plan-form integrations and in the derivation and presentation of velocity potentials and pressures, the conventional analysis system shown in figure 2(a) is utilized. In order to maintain the usual stability system of positive forces and moments, the axes systems shown in figures 2(b) and 2(c) are used in formulating the stability derivatives. A table of transformation formulas is provided which enables the stability derivatives, presented herein with reference to a center of gravity (origin) located at the leading edge of the root chord (fig. 2(b)), to be obtained with reference to an arbitrary center-of-gravity location (fig. 2(c)).

Basic Considerations

The calculation of forces acting on the vertical tail essentially requires a knowledge of the distribution of the pressure difference between the two sides of the tail surface. This pressure-difference distribution is expressible in terms of the perturbation-velocity-potential difference or "potential jump across the surface" $\Delta\varphi$ by means of the linearized relationship

$$\frac{\Delta p}{q} = \frac{2}{V^2}\left(V\frac{\partial}{\partial x}\Delta\varphi + \frac{\partial}{\partial t}\Delta\varphi\right) \tag{1}$$

Inasmuch as for the present investigation thin isolated tail surfaces are considered and thus no induced effects are present from any neighboring surface, the perturbation velocity potentials on the two sides of the tail are equal in magnitude but are of opposite sign. Equation (1) may then be rewritten in terms of the perturbation velocity potential φ as follows:

$$\frac{\Delta p}{q} = -\frac{4}{V^2}\left(V\frac{\partial\varphi}{\partial x} + \frac{\partial\varphi}{\partial t}\right) \tag{2}$$

where φ is evaluated on the negative y-side of the tail surface.

The basic problem, then, is to find for each motion under consideration the perturbation-velocity-potential function φ for the various tail regional areas formed by plan-form and Mach line boundaries. (See, for example, the sketch given in table I.)

For time-independent motions, such as steady rolling, steady yawing, and constant sideslip, the potential functions are of course independent of time (i.e., the last term in eqs. (1) and (2) vanishes) and may be determined by the well-known source-distribution method utilizing the area-cancellation—Mach line reflection technique of reference 11. The mathematical details are not presented herein, because it is felt that previous papers dealing with wing problems (e.g., refs. 12 to 15) have applied the basic method in sufficient detail. The main difference to be noted is that the root chord of the isolated vertical tail is, in effect, another free subsonic edge similar to the tip chord and must be treated accordingly. Actually, tail regions I and III (refer to the sketch in table I) are not affected by the additional tip, and wing results in these regions for constant angle of attack (ref. 15), steady rolling (ref. 15), and steady pitching motion (ref. 13) are applicable to constant sideslip, steady rolling, and steady yawing motions, respectively, for the vertical tail, provided appropriate changes in coordinates are introduced and the proper sign convention is maintained.

The time-dependent motion considered in the present paper, that is, constant lateral acceleration, can be analyzed in a manner analogous to that used for a wing surface undergoing constant vertical acceleration (e.g., refs. 16 to 18). By following this procedure, the basic expressions for the perturbation velocity potential and pressure coefficient (evaluated at time $t = 0$) may be derived as follows:

$$\varphi = -\dot{\beta}\left[\frac{M^2}{B^2}\varphi_{r=1} - \left(t - \frac{M^2x}{B^2V}\right)\varphi_{\beta=1}\right] \tag{3}$$

$$\frac{\Delta P}{q} = -\frac{\dot{\beta}}{B^2}\left[M^2\left(\frac{\Delta P}{q}\right)_{r=1} + \frac{M^2x}{V}\left(\frac{\Delta P}{q}\right)_{\beta=1} - \frac{4}{V^2}\varphi_{\beta=1}\right] \tag{4}$$

Equations (3) and (4) may be deduced directly from equations (1) and (2) of reference 18, provided the corresponding tail motion is substituted for each wing motion and, further, that care is exercised in preserving the conventional system of positive forces and moments. The choice of time $t = 0$ in equation (4) was made for purposes of convenience and simplicity, inasmuch as the pressure due to constant sideslip is eliminated, and thus only the increment in pressure due to time rate of change of sideslip, that is, $\dot{\beta}$, remains.

The right-hand sides of equations (3) and (4) are composed of terms involving steady or time-independent motions, in particular, the motions previously discussed in this section. Thus, once the potentials and pressures are determined for steady yawing and constant sideslip, corresponding expressions may be obtained for constant lateral acceleration by use of equations (3) and (4).

Derivation of the potentials and pressures for the various regions of the general tail plan form under consideration have been carried out for each motion by using the methods and techniques discussed. Tabulations of the potential and pressure-distribution functions are given in tables I and II for constant sideslip, in tables III and IV for steady rolling, in tables V and VI for steady yawing, and in tables VII and VIII for constant lateral acceleration.

The forces and moments acting on the vertical tail due to each motion may be obtained by plan-form integrations of the appropriate potential and pressure functions and may be given as follows (the center of gravity is assumed to be at the leading edge of the root section):

$$Y = q \int_{\text{Root}}^{\text{Tip}} \int_{\text{L.E.}}^{\text{T.E.}} \frac{\Delta P}{q} \, dx \, dz \tag{5}$$

$$N = -q \int_{\text{Root}}^{\text{Tip}} \int_{\text{L.E.}}^{\text{T.E.}} \frac{\Delta P}{q} \, x \, dx \, dz \tag{6}$$

$$L' = q \int_{\text{Root}}^{\text{Tip}} \int_{\text{L.E.}}^{\text{T.E.}} \frac{\Delta P}{q} \, z \, dx \, dz \tag{7}$$

For steady motions, $\frac{\Delta P}{q} = -\frac{4}{V} \frac{\partial \Phi}{\partial x}$ and thus the first integration with respect to x in equations (5) and (7) yields φ; hence, equations (5) and (7), when applied to steady motions, reduce to essentially a single integration involving the potential function.

The nondimensional force and moment coefficients and corresponding stability derivatives are directly obtainable from the definitions given in the list of symbols. For example,

$$C_{n_r} = \left(\frac{\partial C_n}{\partial \frac{rb}{V}} \right)_{r \to 0}$$

$$= \left[\frac{\partial}{\partial \frac{rb}{V}} \left(\frac{N}{qSb} \right) \right]_{r \to 0}$$

$$= \left[\frac{\partial}{\partial \frac{rb}{V}} \left(-\frac{1}{Sb} \int_{\text{Root}}^{\text{Tip}} \int_{\text{L.E.}}^{\text{T.E.}} \frac{\Delta P}{q} \, x \, dx \, dz \right) \right]_{r \to 0}$$

Inasmuch as the various pressure coefficients are linear with reference to their respective angular velocities, attitude, or acceleration (i.e., linear in p, r, β, or $\dot{\beta}$), the partial derivative in the preceding example may be replaced by $\frac{1}{rb/V}$ and the derivative C_{n_r} is then expressed as

$$C_{n_r} = -\frac{1}{Sb^2 \frac{r}{V}} \int_{\text{Root}}^{\text{Tip}} \int_{\text{L.E.}}^{\text{T.E.}} \frac{\Delta P}{q} x \, dx \, dz \tag{8}$$

Corresponding expressions for the 11 other derivatives C_{Y_β}, C_{n_β}, C_{l_β}, C_{Y_r}, C_{l_r}, C_{Y_p}, C_{n_p}, C_{l_p}, $C_{Y_{\dot{\beta}}}$, $C_{n_{\dot{\beta}}}$, and $C_{l_{\dot{\beta}}}$ may be obtained in an analogous manner.

In the present paper, the triangular vertical tail with unswept trailing edge (half-delta) and the rectangular vertical tail have been analyzed in detail. The results obtained upon performing the plan-form integrations and other mathematical operations indicated in the previous discussion are tabulated in table IX. For convenience, a table of transformation formulas is presented (table X) which enables the derived results for the stability derivatives (table IX) to be expressed with respect to an arbitrary center-of-gravity location.

COMPUTATIONAL RESULTS AND DISCUSSION

The formulas for the stability derivatives given in table IX are seen to be functions of the tail aspect ratio A and the Mach number parameter $B = \sqrt{M^2 - 1}$. Use of the combined parameter AB as the abscissa variable and appropriate choice of derivative parameters as the ordinates allow the analytical results for most of the stability derivatives to be expressed graphically by means of a single simple curve; the stability derivatives due to $\dot{\beta}$-motion require two curves. Figures 3 to 8 present the results for the half-delta tail and figures 9 to 13 present the analogous results for the rectangular tail. The lower limit $AB = 2$ for the half-delta vertical tail corresponds to the sonic-leading-edge condition; values of $AB < 2$, for which the tail leading edge is subsonic, are considered in reference 10. The lower limit $AB = 1$ for the rectangular vertical tail corresponds to the condition where the Mach line from the leading edge of the root chord intersects the trailing edge of the tip chord. Calculation of the derivatives for the situation where the Mach line from the leading edge of the root chord intersects the tip chord, that is, values of $AB < 1$, cannot, in general, be obtained easily because of the fact that

the calculation involves the consideration of interacting external flow fields. The lower limit $AB = 1$ in this case is not very restrictive except for very low aspect ratios at low supersonic Mach numbers.

In considering the curves given in figures 3 to 13, the following facts should be kept in mind: (a) The results are for a completely isolated vertical tail, (b) the center-of-gravity location is assumed to be at the tail apex, and (c) parameters used for nondimensionalizing purposes are the area and span of the vertical tail. For other center-of-gravity locations, analogous curves may be drawn by use of the presented data and the axes-transformation formulas given in table X.

Thus far, only the isolated vertical tail has been considered, that is, the zero-end-plate solution. For comparison purposes, results for several of the derivatives based on a complete-end-plate analysis have been obtained and are presented in figures 14 and 15. The comparisons are shown for the side-force and yawing-moment derivatives due to constant sideslip, steady yawing, and constant lateral acceleration. The complete-end-plate results for these tail derivatives are obtainable from stability derivatives previously reported for symmetrical wings (refs. 13, 15, and 18), provided modifications are introduced to account for (a) changes in nondimensionalizing parameters, (b) correspondence of wing and vertical-tail motions, and (c) preservation of sign convention for positive sense of motion, moments, and so forth. The transformations of symmetrical-wing derivatives into complete-end-plate derivatives for vertical tails having the same plan-form geometry as the half-wing may be summarized as follows:

$$\text{Expression for } C_{Y_\beta} = -1\left(\begin{array}{c}\text{Expression for } C_{L_\alpha} \text{ with wing}\\ \text{aspect ratio replaced by } 2A\end{array}\right)$$

$$\text{Expression for } C_{n_\beta} = -\frac{4}{3A}\frac{1+\lambda+\lambda^2}{(1+\lambda)^2}\left(\begin{array}{c}\text{Expression for } C_{m_\alpha} \text{ with wing}\\ \text{aspect ratio replaced by } 2A\end{array}\right)$$

$$\text{Expression for } C_{Y_r} = \frac{2}{3A}\frac{1+\lambda+\lambda^2}{(1+\lambda)^2}\left(\begin{array}{c}\text{Expression for } C_{L_q} \text{ with wing}\\ \text{aspect ratio replaced by } 2A\end{array}\right)$$

$$\text{Expression for } C_{n_r} = \frac{8}{9A^2}\frac{(1+\lambda+\lambda^2)^2}{(1+\lambda)^4}\left(\begin{array}{c}\text{Expression for } C_{m_q} \text{ with wing}\\ \text{aspect ratio replaced by } 2A\end{array}\right)$$

$$\text{Expression for } C_{Y_{\dot\beta}} = -\frac{2}{3A}\frac{1+\lambda+\lambda^2}{(1+\lambda)^2}\left(\begin{array}{c}\text{Expression for } C_{L_{\dot\alpha}} \text{ with wing}\\ \text{aspect ratio replaced by } 2A\end{array}\right)$$

$$\text{Expression for } C_{n_{\dot{\beta}}} = -\frac{8}{9A^2}\frac{(1+\lambda+\lambda^2)^2}{(1+\lambda)^4}\left(\begin{array}{l}\text{Expression for } C_{m_{\dot{\alpha}}} \text{ with wing}\\ \text{aspect ratio replaced by } 2A\end{array}\right)$$

where C_{L_α}, C_{m_α}, C_{L_q}, C_{m_q}, $C_{L_{\dot{\alpha}}}$, and $C_{m_{\dot{\alpha}}}$ are conventionally defined wing derivatives (see, for example, p. 5 of ref. 18). For completeness, previously reported results (ref. 10) for the half-delta vertical tail with subsonic leading edges (i.e., $AB < 2$) are included in figure 14. Figures 14 and 15 indicate that for a given aspect ratio the effect of an end plate decreases with increasing Mach number and that for a given Mach number the effect of an end plate decreases with increasing aspect ratio. Although these conclusions apply specifically to those derivatives presented, it is felt that similar evidence would be found for the other derivatives as well. The percentage differences between zero- and complete-end-plate results vary of course with center-of-gravity location, as well as with Mach number and aspect ratio, but in general are not too large for the side-force and yawing-moment derivatives considered except at the lower values of AB.

It should be remembered that the derivatives as presented herein have been made nondimensional with respect to vertical-tail parameters such as tail span b, tail area S, and the angles pb/V, rb/V, and $\dot{\beta}b/V$. The magnitudes of the derivatives may, therefore, appear to be quite large with respect to the expected tail contributions to the derivatives for a complete airplane. The following factors should be used in converting the presented analytical and numerical results to corresponding derivatives (denoted in the following relationships by subscript w) based on wing area S_w, wing span b_w, and angles $pb_w/2V$, $rb_w/2V$, and $\dot{\beta}b_w/2V$:

$$\left(C_{Y_\beta}\right)_w = \frac{S}{S_w} C_{Y_\beta}$$

$$\left(C_{n_\beta}\right)_w,\ \left(C_{l_\beta}\right)_w = \frac{S}{S_w}\frac{b}{b_w}\left(C_{n_\beta},\ C_{l_\beta}\right)$$

$$\left(C_{Y_p}\right)_w,\ \left(C_{Y_r}\right)_w,\ \left(C_{Y_{\dot{\beta}}}\right)_w = 2\frac{S}{S_w}\frac{b}{b_w}\left(C_{Y_p},\ C_{Y_r},\ C_{Y_{\dot{\beta}}}\right)$$

$$\left(C_{n_p}\right)_w,\ \left(C_{l_p}\right)_w,\ \left(C_{n_r}\right)_w,\ \left(C_{l_r}\right)_w,\ \left(C_{n_{\dot{\beta}}}\right)_w,\ \left(C_{l_{\dot{\beta}}}\right)_w =$$

$$2\frac{S}{S_w}\left(\frac{b}{b_w}\right)^2\left(C_{n_p},\ C_{l_p},\ C_{n_r},\ C_{l_r},\ C_{n_{\dot{\beta}}},\ C_{l_{\dot{\beta}}}\right)$$

CONCLUDING REMARKS

Expressions based on the application of linearized thin-airfoil theory for supersonic speeds have been derived for the velocity potentials and pressure distributions due to various lateral motions for a family of thin isolated vertical tails of arbitrary sweepback and taper ratio. Motions considered were steady rolling, steady yawing, and constant lateral acceleration. Forces and moments, expressed in the form of stability derivatives, were presented for the rectangular and half-delta vertical tails. The results are, in general, applicable at those supersonic speeds for which both the tail leading and trailing edges are supersonic. For purposes of completeness, analogous results for sideslip motion obtained primarily from other sources have been included.

The effects of a complete end plate on several of the side-force and yawing-moment derivatives have been considered, and it appears that only for relatively small values of the aspect-ratio—Mach number parameter $A\sqrt{M^2 - 1}$ do the complete- and zero-end-plate values differ significantly enough to warrant further study of finite-end-plate corrections. This statement may not be applicable for rolling motion, nor is it necessarily true for rolling-moment derivatives in general.

An additional point of interest pertinent to the present investigation is that the results obtained for the yawing-moment derivatives due to steady yawing and constant lateral acceleration C_{n_r} and $C_{n_{\dot{\beta}}}$ may be used to approximate the aerodynamic damping of the lateral oscillation in yaw to the first order in frequency. This approximation to the lateral damping is given by the expression $C_{n_r} - C_{n_{\dot{\beta}}}$ and can be rapidly calculated from the curves and formulas given herein.

Langley Aeronautical Laboratory,
National Advisory Committee for Aeronautics,
Langley Field, Va., December 16, 1954.

REFERENCES

1. Lomax, Harvard, and Heaslet, Max. A.: Damping-in-Roll Calculations for Slender Swept-Back Wings and Slender Wing-Body Combinations. NACA TN 1950, 1949.

2. Adams, Gaynor J.: Theoretical Damping in Roll and Rolling Effectiveness of Slender Cruciform Wings. NACA TN 2270, 1951.

3. Bobbitt, Percy J., and Malvestuto, Frank S., Jr.: Estimation of Forces and Moments Due to Rolling for Several Slender-Tail Configurations at Supersonic Speeds. NACA TN 2955, 1953.

4. Ribner, Herbert S.: Damping in Roll of Cruciform and Some Related Delta Wings at Supersonic Speeds. NACA TN 2285, 1951.

5. Spreiter, John R.: The Aerodynamic Forces on Slender Plane- and Cruciform-Wing and Body Combinations. NACA Rep. 962, 1950. (Supersedes NACA TN's 1897 and 1662.)

6. Bryson, Arthur E., Jr.: Stability Derivatives for a Slender Missile With Application to a Wing-Body-Vertical-Tail Configuration. Jour. Aero. Sci., vol. 20, no. 5, May 1953, pp. 297-308.

7. Sacks, Alvin H.: Aerodynamic Forces, Moments, and Stability Derivatives for Slender Bodies of General Cross Section. NACA TN 3283, 1954.

8. Martin, John C., and Malvestuto, Frank S., Jr.: Theoretical Force and Moments Due to Sideslip of a Number of Vertical Tail Configurations at Supersonic Speeds. NACA TN 2412, 1951.

9. Malvestuto, Frank S., Jr.: Theoretical Supersonic Force and Moment Coefficients on a Sideslipping Vertical- and Horizontal-Tail Combination With Subsonic Leading Edges and Supersonic Trailing Edges. NACA TN 3071, 1954.

10. Bobbitt, Percy J.: Theoretical Calculations of the Lateral Stability Derivatives for Triangular Vertical Tails With Subsonic Leading Edges Traveling at Supersonic Speeds. NACA TN 3240, 1954.

11. Evvard, John C.: Distribution of Wave Drag and Lift in the Vicinity of Wing Tips at Supersonic Speeds. NACA TN 1382, 1947.

12. Malvestuto, Frank S., Jr., Margolis, Kenneth, and Ribner, Herbert S.: Theoretical Lift and Damping in Roll at Supersonic Speeds of Thin Sweptback Tapered Wings With Streamwise Tips, Subsonic Leading Edges, and Supersonic Trailing Edges. NACA Rep. 970, 1950. (Supersedes NACA TN 1860.)

13. Martin, John C., Margolis, Kenneth, and Jeffreys, Isabella: Calculation of Lift and Pitching Moments Due to Angle of Attack and Steady Pitching Velocity at Supersonic Speeds for Thin Sweptback Tapered Wings With Streamwise Tips and Supersonic Leading and Trailing Edges. NACA TN 2699, 1952.

14. Margolis, Kenneth, Sherman, Windsor L., and Hannah, Margery E.: Theoretical Calculation of the Pressure Distribution, Span Loading, and Rolling Moment Due to Sideslip at Supersonic Speeds for Thin Sweptback Tapered Wings With Supersonic Trailing Edges and Wing Tips Parallel to the Axis of Wing Symmetry. NACA TN 2898, 1953.

15. Harmon, Sidney M., and Jeffreys, Isabella: Theoretical Lift and Damping in Roll of Thin Wings With Arbitrary Sweep and Taper at Supersonic Speeds - Supersonic Leading and Trailing Edges. NACA TN 2114, 1950.

16. Ribner, Herbert S., and Malvestuto, Frank S., Jr.: Stability Derivatives of Triangular Wings at Supersonic Speeds. NACA Rep. 908, 1948. (Supersedes NACA TN 1572.)

17. Malvestuto, Frank S., Jr., and Hoover, Dorothy M.: Supersonic Lift and Pitching Moment of Thin Sweptback Tapered Wings Produced by Constant Vertical Acceleration - Subsonic Leading Edges and Supersonic Trailing Edges. NACA TN 2315, 1951.

18. Cole, Isabella J., and Margolis, Kenneth: Lift and Pitching Moment at Supersonic Speeds Due to Constant Vertical Acceleration for Thin Sweptback Tapered Wings With Streamwise Tips - Supersonic Leading and Trailing Edges. NACA TN 3196, 1954.

TABLE I

FORMULAS FOR POTENTIAL DISTRIBUTION DUE TO CONSTANT SIDESLIP

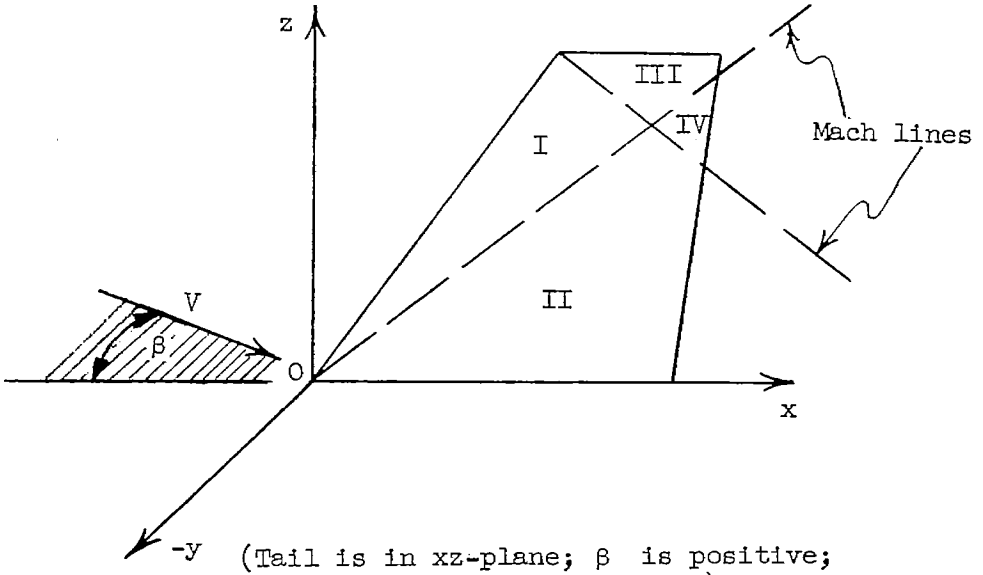

(Tail is in xz-plane; β is positive; V as shown is in xy-plane)

Region (see sketch)	$\varphi(x,0^-,z)$
I	$\dfrac{V\beta(mx - z)}{\sqrt{B^2m^2 - 1}}$
II	$\dfrac{V\beta}{\pi\sqrt{B^2m^2 - 1}}\left[(mx - z)\cos^{-1}\dfrac{mx - z(2Bm - 1)}{mx - z} + 2\sqrt{zm(x - Bz)(Bm - 1)}\right]$
III	$\dfrac{V\beta}{\pi\sqrt{B^2m^2 - 1}}\left\{(mx - z)\cos^{-1}\dfrac{mx - z + 2(1 + Bm)(z - b)}{mx - z} + 2\sqrt{(z - b)(Bm + 1)\left[b(1 + Bm) - m(x + Bz)\right]}\right\}$
IV	$\sum$ (II + III - I)

TABLE II

FORMULAS FOR PRESSURE-DIFFERENCE COEFFICIENT DUE TO CONSTANT SIDESLIP

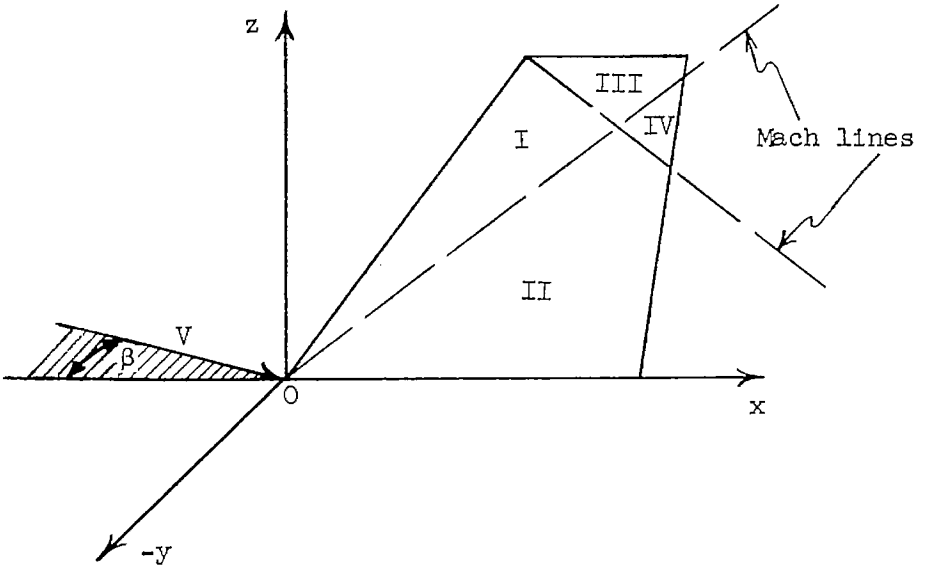

(Tail is in xz-plane; β is positive;
V as shown is in xy-plane)

Region (see sketch)	$\frac{\Delta P}{q}(x,z)$
I	$-\frac{4\beta m}{\sqrt{B^2m^2-1}}$
II	$-\frac{4\beta m}{\pi\sqrt{B^2m^2-1}}\cos^{-1}\frac{mx-z(2Bm-1)}{mx-z}$
III	$-\frac{4\beta m}{\pi\sqrt{B^2m^2-1}}\cos^{-1}\frac{mx-z+2(1+Bm)(z-b)}{mx-z}$
IV	$\sum(\text{II}+\text{III}-\text{I})$

TABLE III

FORMULAS FOR POTENTIAL DISTRIBUTION DUE TO STEADY ROLLING

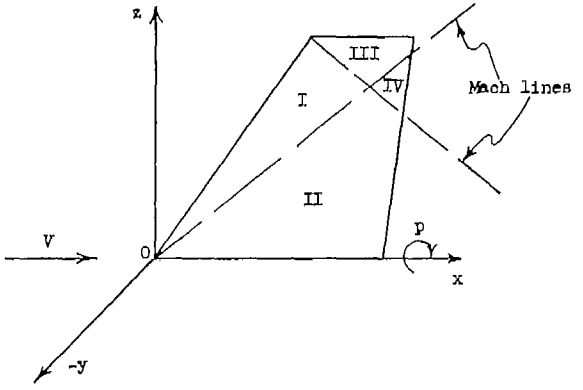

(Tail is in xz-plane; positive rolling)

Region (see sketch)	$\varphi(x,0^-,z)$
I	$\frac{p}{2(B^2m^2-1)^{3/2}}\left\{(mx-z)\left[-mx+z(2B^2m^2-1)\right]\right\}$
II	$\frac{p}{\pi}\left\{\frac{mx(4Bm-1)+z(2B^2m^2-2Bm-3)}{3(B^2m^2-1)}\sqrt{\frac{mz(x-Bz)}{Bm+1}}-\frac{(mx-z)\left[mx-z(2B^2m^2-1)\right]}{2(B^2m^2-1)^{3/2}}\cos^{-1}\frac{mx+z(1-2Bm)}{mx-z}\right\}$
III	$\frac{p}{\pi(B^2m^2-1)^{3/2}}\left\{\frac{(mx-z)\left[-mx+z(2B^2m^2-1)\right]}{2}\cos^{-1}\frac{mx-z+2(1+Bm)(z-b)}{mx-z}-\frac{(mx-b)(4Bm-1)+(z-b)(3-2B^2m^2-2Bm)}{3}-6b(B^2m^2-1)\sqrt{(z-b)(Bm+1)\left[b(1+Bm)-m(x+Bz)\right]}\right\}$
IV	$\sum(\text{II}+\text{III}-\text{I})$

TABLE IV

FORMULAS FOR PRESSURE-DIFFERENCE COEFFICIENT DUE TO STEADY ROLLING

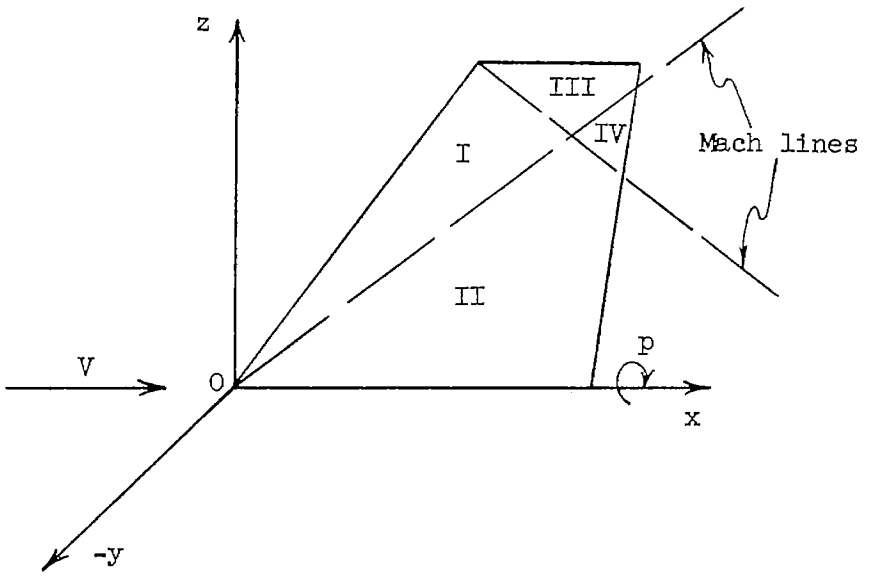

(Tail is in xz-plane; positive rolling)

Region (see sketch)	$\frac{\Delta P}{q}(x,z)$
I	$-\frac{4pm(B^2m^2z - mx)}{V(B^2m^2 - 1)^{3/2}}$
II	$-\frac{4p}{\pi V}\left[\frac{2Bm^2}{(B^2m^2 - 1)}\sqrt{\frac{zm(x - Bz)}{Bm + 1}} - \frac{m^2(x - B^2zm)}{(B^2m^2 - 1)^{3/2}}\cos^{-1}\frac{mx + z(1 - 2Bm)}{mx - z}\right]$
III	$-\frac{4pm}{\pi V(B^2m^2 - 1)^{3/2}}\left\{(B^2m^2z - mx)\cos^{-1}\frac{mx - z + 2(1 + Bm)(z - b)}{mx - z} - 2Bm\sqrt{(z - b)(Bm + 1)\left[b(1 + Bm) - m(x + Bz)\right]}\right\}$
IV	$\sum(\text{II} + \text{III} - \text{I})$

TABLE V

FORMULAS FOR POTENTIAL DISTRIBUTION DUE TO STEADY YAWING

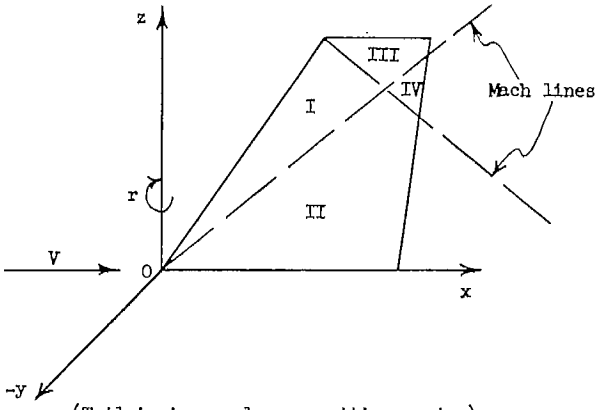

(Tail is in xz-plane; positive yawing)

Region (see sketch)	$\varphi(x,0^-,z)$
I	$-\frac{r}{2(B^2m^2-1)^{3/2}}\left[x^2\left(-2m+B^2m^3\right)+2xz-B^2z^2m\right]$
II	$-\frac{r}{\pi}\left\{\frac{x(5B^2m^2+4Bm-6)-B^2mz(2Bm+1)}{3(B^2m^2-1)}\sqrt{\frac{mz(x-Bz)}{Bm+1}}+\frac{(mx-z)\left[mzB^2+x(m^2B^2-2)\right]}{2(B^2m^2-1)^{3/2}}\cos^{-1}\frac{mx-z(2Bm-1)}{mx-z}\right\}$
III	$-\frac{r}{\pi}\left\{\frac{mx(5B^2m^2-4Bm-6)+B^2m^2(z-b)(2Bm-1)+Bmb(4+Bm)}{3m(B^2m^2-1)^{3/2}}\sqrt{(z-b)(Bm+1)\left[b(1+Bm)-m(x+Bz)\right]}+\frac{(mx-z)\left[B^2m^2(mx+z)-2mx\right]}{2m(B^2m^2-1)^{3/2}}\cos^{-1}\frac{mx-z+2(1+Bm)(z-b)}{mx-z}\right\}$
IV	$\sum(\text{II}+\text{III}-\text{I})$

TABLE VI

FORMULAS FOR PRESSURE-DIFFERENCE COEFFICIENT DUE TO STEADY YAWING

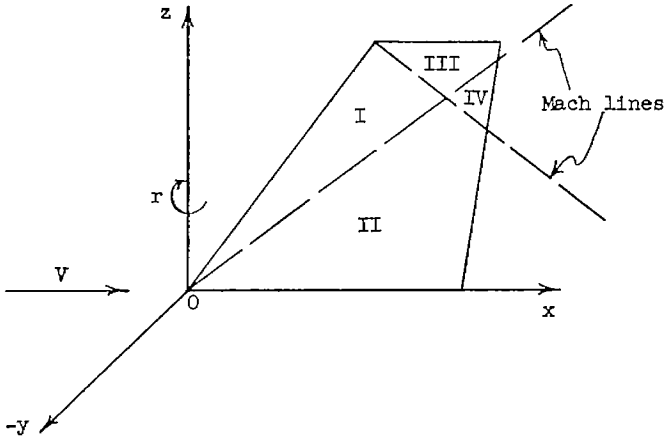

(Tail is in xz-plane; positive yawing)

Region (see sketch)	$\frac{\Delta p}{q}(x,z)$
I	$\frac{2r}{V(B^2m^2-1)^{3/2}}\left[2mx(B^2m^2-2)+2z\right]$
II	$\frac{4r}{\pi V(B^2m^2-1)^{3/2}}\left\{\left[mx(B^2m^2-2)+z\right]\cos^{-1}\frac{mx-z(2Bm-1)}{mx-z}+2(B^2m^2+Bm-1)\sqrt{mz(Bm-1)(x-Bz)}\right\}$
III	$\frac{4r}{\pi V(B^2m^2-1)^{3/2}}\left\{\left[z+mx(B^2m^2-2)\right]\cos^{-1}\frac{mx-z+2(1+Bm)(z-b)}{mx-z}+2(B^2m^2-Bm-1)\sqrt{(z-b)(Bm+1)\left[b(1+Bm)-m(x+Bz)\right]}\right\}$
IV	$\sum$ (II + III - I)

TABLE VII

FORMULAS FOR POTENTIAL DISTRIBUTION DUE TO CONSTANT LATERAL ACCELERATION

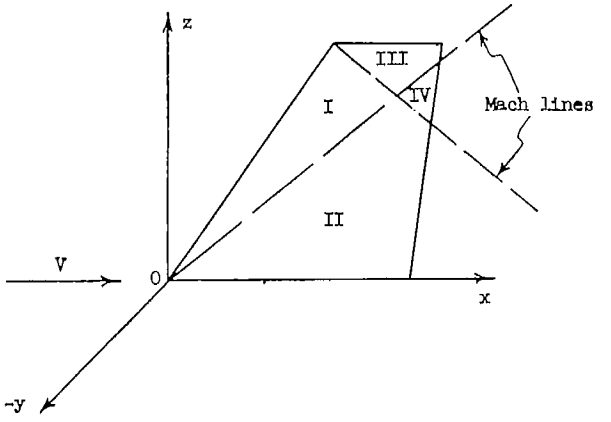

(Tail is in xz-plane; positive $\dot{\beta}$ in positive y-direction)

Region (see sketch)	$\varphi(x,0^-,z)$
I	$\frac{\dot{\beta}(mx - z)}{\sqrt{B^2m^2 - 1}}\left[tV - \frac{mM^2(mx - z)}{2(B^2m^2 - 1)}\right]$
II	$\frac{\dot{\beta}}{\pi\sqrt{B^2m^2 - 1}}\left\{\sqrt{mz(x - Bz)(Bm - 1)}\left[2tV + \frac{M^2mx(4 - Bm) - M^2mBz(2Bm + 1)}{3B(B^2m^2 - 1)}\right] + \left[\cos^{-1}\frac{mx - z(2Bm - 1)}{mx - z}\right]\left[\frac{M^2m(z - mx)}{2(B^2m^2 - 1)} + tV\right](mx - z)\right\}$
III	$\frac{\dot{\beta}}{\pi\sqrt{B^2m^2 - 1}}\left\{\sqrt{(z - b)(Bm + 1)\left[b(1 + Bm) - m(x + Bz)\right]}\left[2tV + \frac{M^2(4 + Bm)(b - mx) + M^2Bm(z - b)(2Bm - 1)}{3B(B^2m^2 - 1)}\right] + \left[\cos^{-1}\frac{mx - z + 2(1 + Bm)(z - b)}{mx - z}\right]\left[tV + \frac{M^2m(z - mx)}{2(B^2m^2 - 1)}\right](mx - z)\right\}$
IV	$\sum$ (II + III - I)

TABLE VIII

FORMULAS FOR PRESSURE-DIFFERENCE COEFFICIENT DUE TO CONSTANT LATERAL ACCELERATION

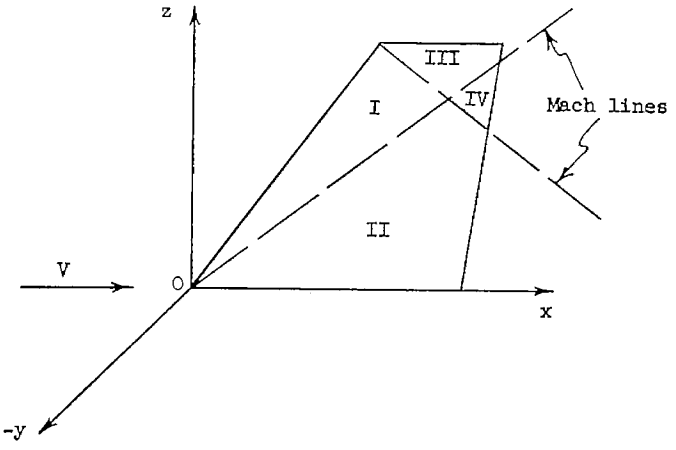

(Tail is in xz-plane; positive $\dot{\beta}$ in positive y-direction)

Region (see sketch)	$\frac{\Delta p}{q}(x,z)$
I	$\frac{4\dot{\beta}(mx - z)(1 + m^2)}{V(B^2m^2 - 1)^{3/2}}$
II	$\frac{4\dot{\beta}}{\pi B^2 V\sqrt{B^2m^2 - 1}}\left\{\frac{B^2(1 + m^2)(mx - z)}{B^2m^2 - 1}\cos^{-1}\frac{mx - z(2Bm - 1)}{mx - z} + 2\left[1 - \frac{M^2(B^2m^2 + Bm - 1)}{B^2m^2 - 1}\right]\sqrt{zm(x - Bz)(Bm - 1)}\right\}$
III	$\frac{4\dot{\beta}}{\pi B^2 V\sqrt{B^2m^2 - 1}}\left\{\frac{B^2(1 + m^2)(mx - z)}{B^2m^2 - 1}\cos^{-1}\frac{mx - z + 2(1 + Bm)(z - b)}{mx - z} + 2\left[1 - \frac{M^2(B^2m^2 - Bm - 1)}{B^2m^2 - 1}\right]\sqrt{(z - b)(Bm + 1)\left[b(1 + Bm) - m(x + Bz)\right]}\right\}$
IV	$\sum$ (II + III - I)

TABLE IX

STABILITY DERIVATIVES FOR HALF-DELTA AND RECTANGULAR ISOLATED VERTICAL TAILS

Derivative (a)	Half-delta tails (b)	Rectangular tails (c)
C_{Y_β}	$-\frac{4}{B}\sqrt{\frac{AB}{AB+2}}$	$-\frac{4}{B}\left(1-\frac{1}{2AB}\right)$
C_{n_β}	$\frac{16}{3AB}\sqrt{\frac{AB}{AB+2}}$	$\frac{2}{AB}\left(1-\frac{2}{3AB}\right)$
C_{l_β}	$-\frac{4}{3B}\frac{AB+1}{\sqrt{AB(AB+2)}}$	$-\frac{2}{B}\left(1-\frac{1}{2AB}\right)$
C_{Y_p}	$-\frac{4}{3B}\frac{\sqrt{AB}(AB+3)}{(AB+2)^{3/2}}$	$-\frac{2AB-1}{AB^2}$
C_{n_p}	$\frac{2(AB+3)}{\sqrt{AB}(AB+2)^{3/2}}$	$\frac{3AB-2}{3A^2B^2}$
C_{l_p}	$-\frac{2A^2B^2+6AB+3}{3B\sqrt{AB}(AB+2)^{3/2}}$	$-\frac{1+4AB-24A^2B^2+32A^3B^3}{24A^3B^4}$
C_{Y_r}	$\frac{8(2AB+5)}{3\sqrt{AB}(AB+2)^{3/2}}$	$\frac{2(3AB-1)}{3A^2B^2}$
C_{n_r}	$-\frac{4B(2AB+5)}{\left[AB(AB+2)\right]^{3/2}}$	$-\frac{B(8AB-3)}{6A^3B^3}$
C_{l_r}	$\frac{2(3A^2B^2+9AB+5)}{3\left[AB(AB+2)\right]^{3/2}}$	$\frac{3AB-1}{3A^2B^2}$
$C_{Y_{\dot\beta}}$	$-\frac{8}{3B^2}\frac{B^2-AB-1}{\sqrt{AB(AB+2)^3}}$	$-\frac{2(B^2+2-3AB)}{3A^2B^4}$
$C_{n_{\dot\beta}}$	$\frac{4}{B}\frac{B^2-AB-1}{\sqrt{A^3B^3(AB+2)^3}}$	$\frac{3B^2-8AB+6}{6A^3B^4}$
$C_{l_{\dot\beta}}$	$\frac{2}{3B^2}\frac{B^2+A^2B^2+3AB+3}{\sqrt{A^3B^3(AB+2)^3}}$	$-\frac{B^2+2-3AB}{3A^2B^4}$

[a]Angular velocities and moments measured about the system of body axes shown in fig. 2(b).

[b]Results valid for $AB \geq 2$.

[c]Results valid for $AB \geq 1$.

TABLE X

TRANSFER-OF-AXES FORMULAS

Stability derivatives in a body system of axes with origin at tail apex (see fig. 2(b))	Formulas for transfer to a body system of axes with origin displaced distances x_o (positive forward) and z_o (positive downward) from the tail apex (see fig. 2(c))
C_{Y_β}	C_{Y_β}
C_{n_β}	$C_{n_\beta} - \frac{x_o}{b} C_{Y_\beta}$
C_{l_β}	$C_{l_\beta} + \frac{z_o}{b} C_{Y_\beta}$
C_{Y_p}	C_{Y_p}
C_{n_p}	$C_{n_p} - \frac{x_o}{b} C_{Y_p}$
C_{l_p}	$C_{l_p} + \frac{z_o}{b} C_{Y_p}$
C_{Y_r}	$C_{Y_r} - \frac{x_o}{b} C_{Y_\beta}$
C_{n_r}	$C_{n_r} - \frac{x_o}{b}\left(C_{n_\beta} + C_{Y_r}\right) + \left(\frac{x_o}{b}\right)^2 C_{Y_\beta}$
C_{l_r}	$C_{l_r} + \frac{z_o}{b} C_{Y_r} - \frac{x_o}{b} C_{l_\beta} - \left(\frac{z_o}{b}\right)\left(\frac{x_o}{b}\right) C_{Y_\beta}$
$C_{Y_{\dot\beta}}$	$C_{Y_{\dot\beta}}$
$C_{n_{\dot\beta}}$	$C_{n_{\dot\beta}} - \frac{x_o}{b} C_{Y_{\dot\beta}}$
$C_{l_{\dot\beta}}$	$C_{l_{\dot\beta}} + \frac{z_o}{b} C_{Y_{\dot\beta}}$

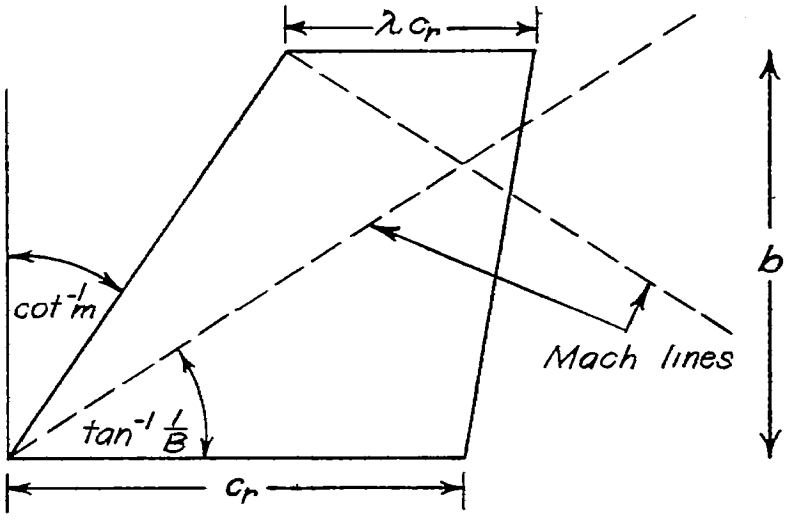

(a) General plan form and pertinent symbols.

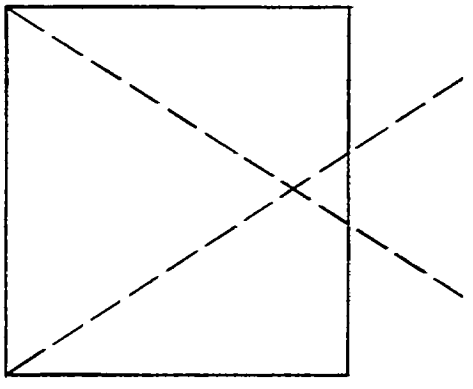

(b) Rectangular tail.

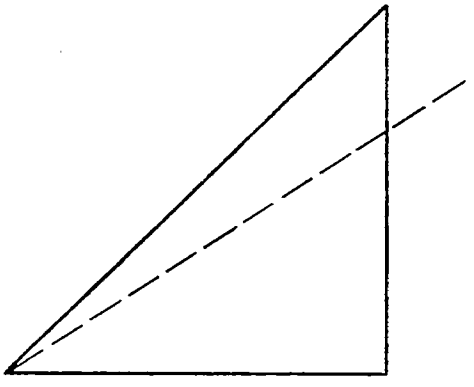

(c) Half-delta tail.

Figure 1.- Tail plan forms and associated data.

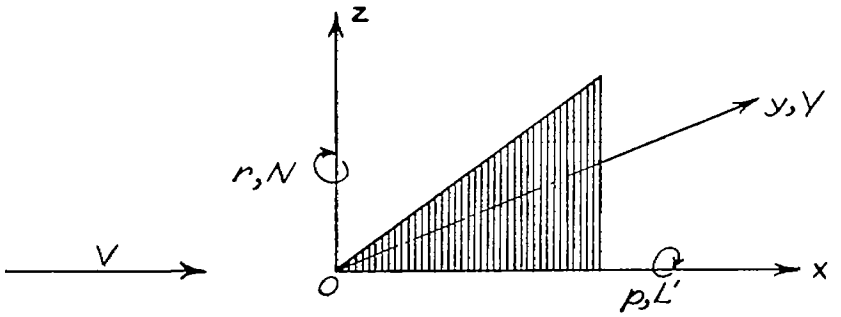

(a) Body-axes system used for analysis. Free-stream velocity V.

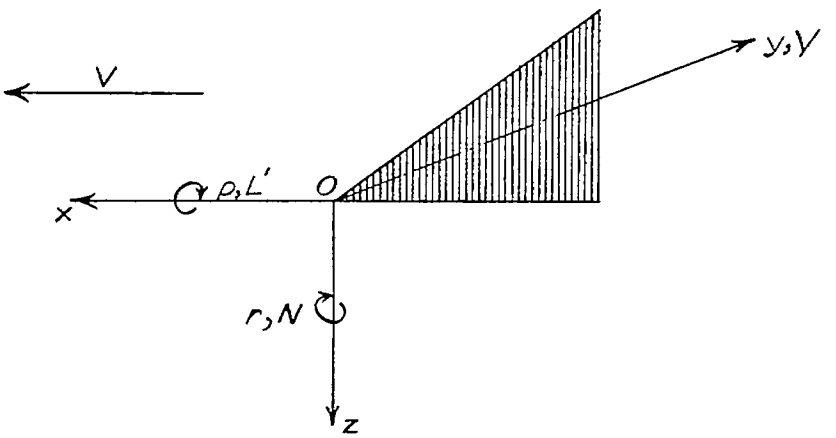

(b) Principal body-axes system used for presentation of stability derivatives. Entire system moving with flight velocity V.

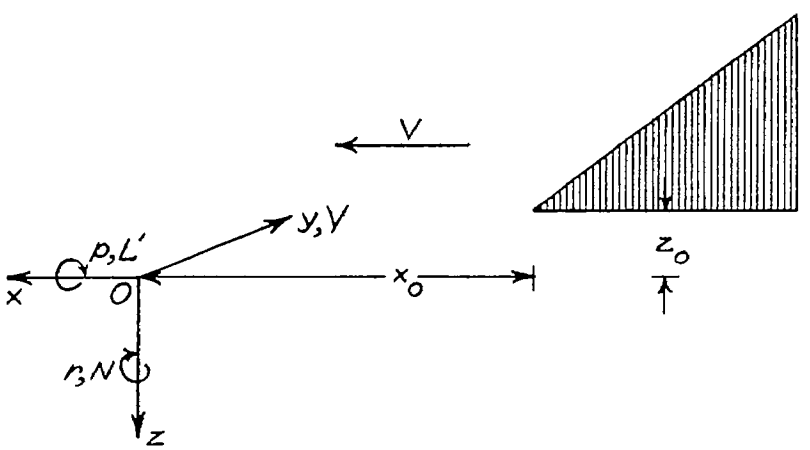

(c) Same type of axes system as (b) with origin translated.

Figure 2.- Systems of body axes. Positive directions of axes, forces, and moments indicated by arrows.

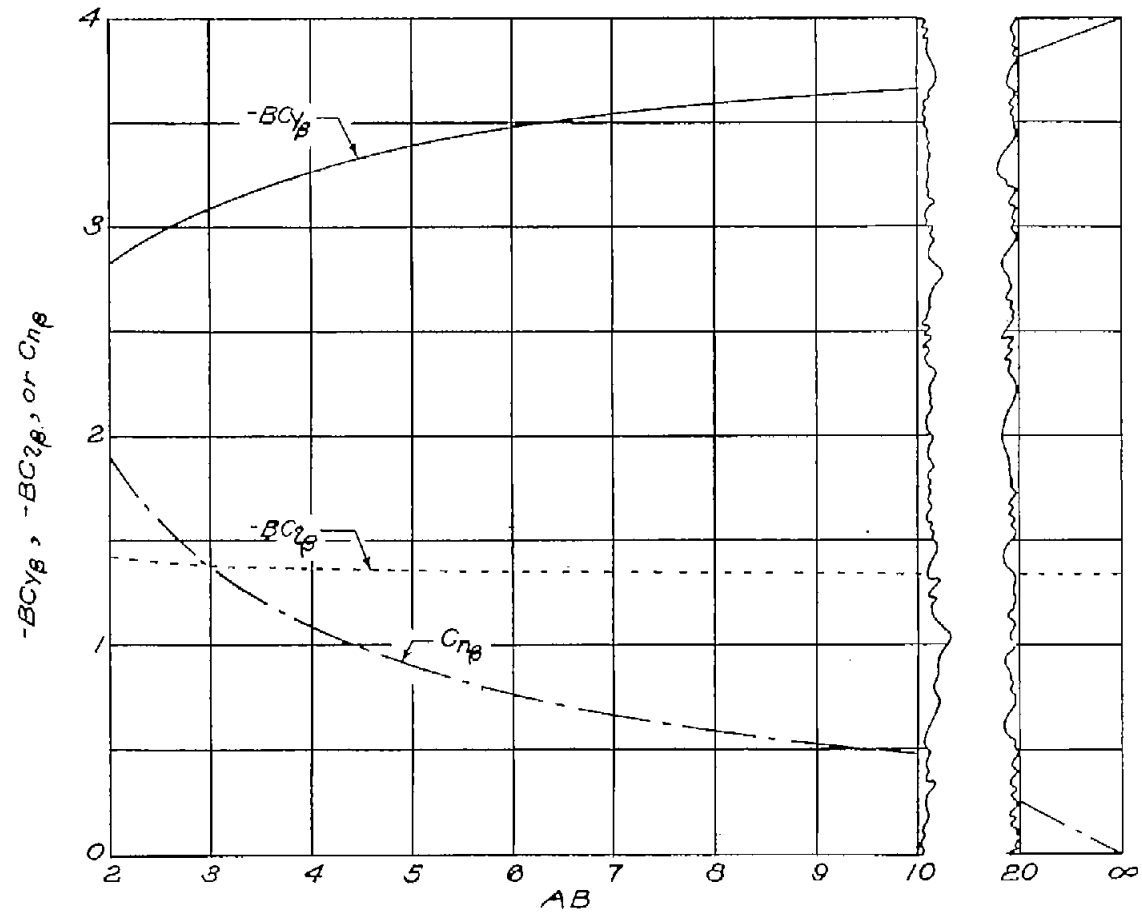

Figure 3.- Curves for determining the stability derivatives due to constant sideslip C_{Y_β}, C_{n_β}, and C_{l_β} for isolated half-delta vertical tails with supersonic leading edges. Derivatives based on vertical-tail parameters b and S; principal body-axes system with origin at leading edge of root section.

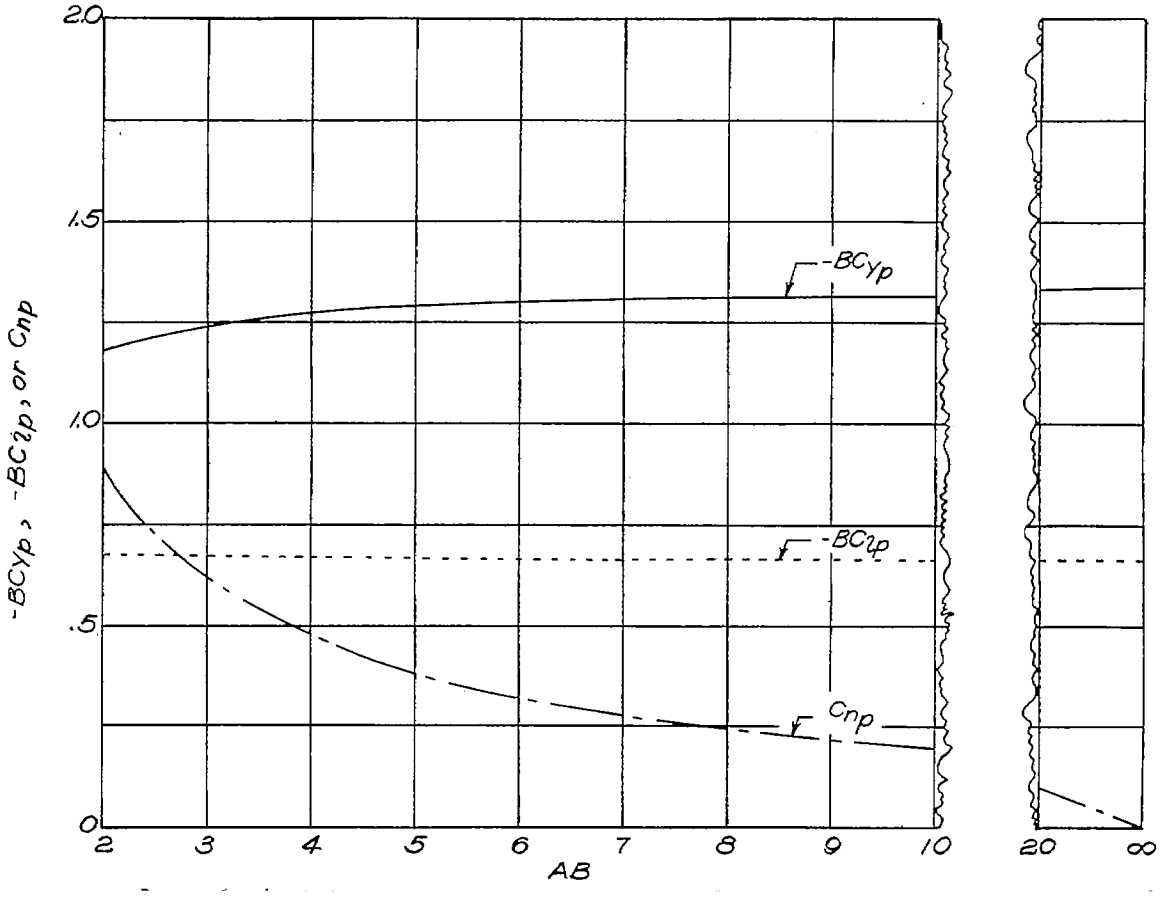

Figure 4.- Curves for determining the stability derivatives due to steady rolling C_{Y_p}, C_{n_p}, and C_{l_p} for isolated half-delta vertical tails with supersonic leading edges. Derivatives based on vertical-tail parameters b, S, and angle pb/V; principal body-axes system with origin at leading edge of root section.

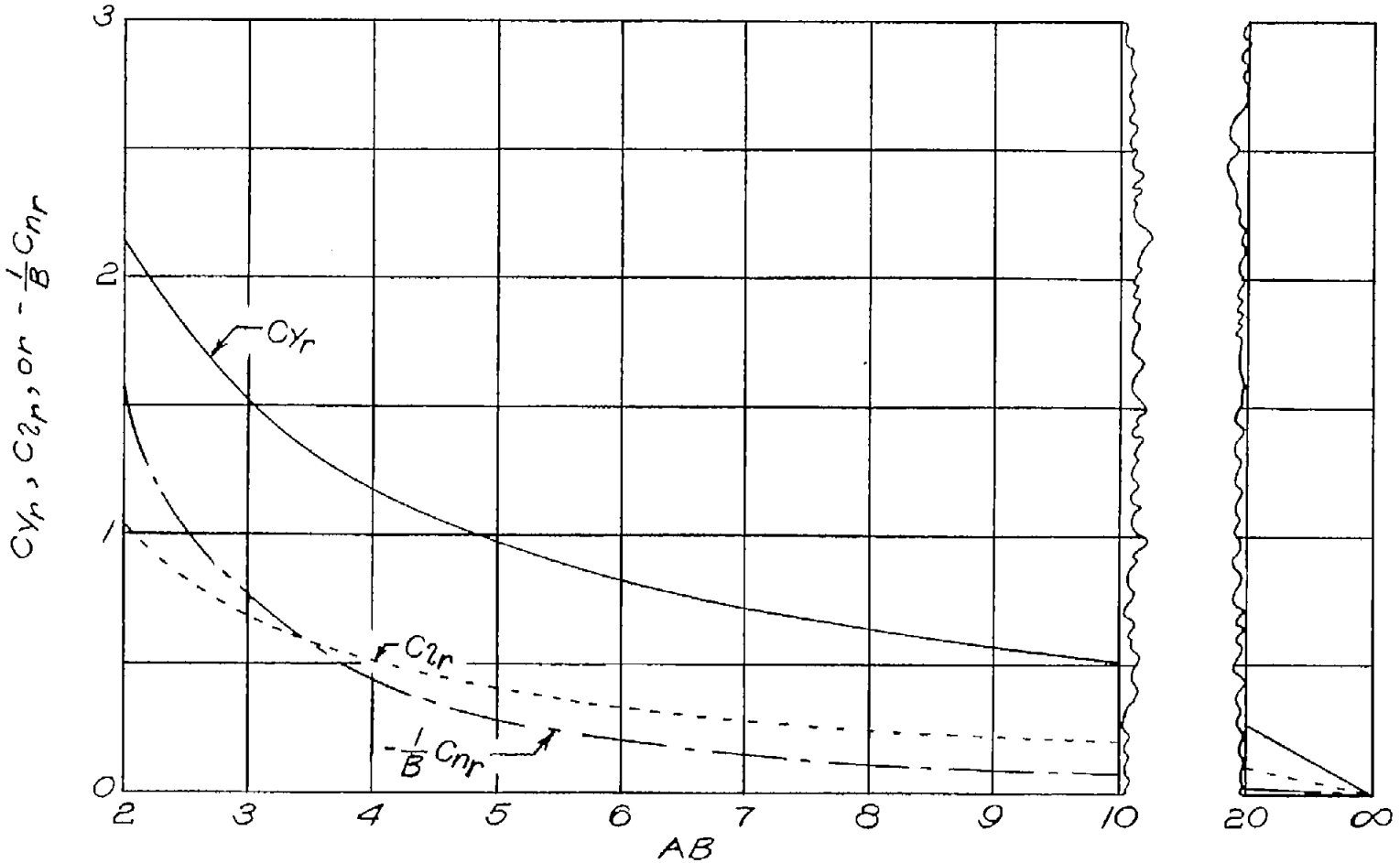

Figure 5.- Curves for determining the stability derivatives due to steady yawing C_{Y_r}, C_{n_r}, and C_{l_r} for isolated half-delta vertical tails with supersonic leading edges. Derivatives based on vertical-tail parameters b, S, and angle rb/V; principal body-axes system with origin at leading edge of root section.

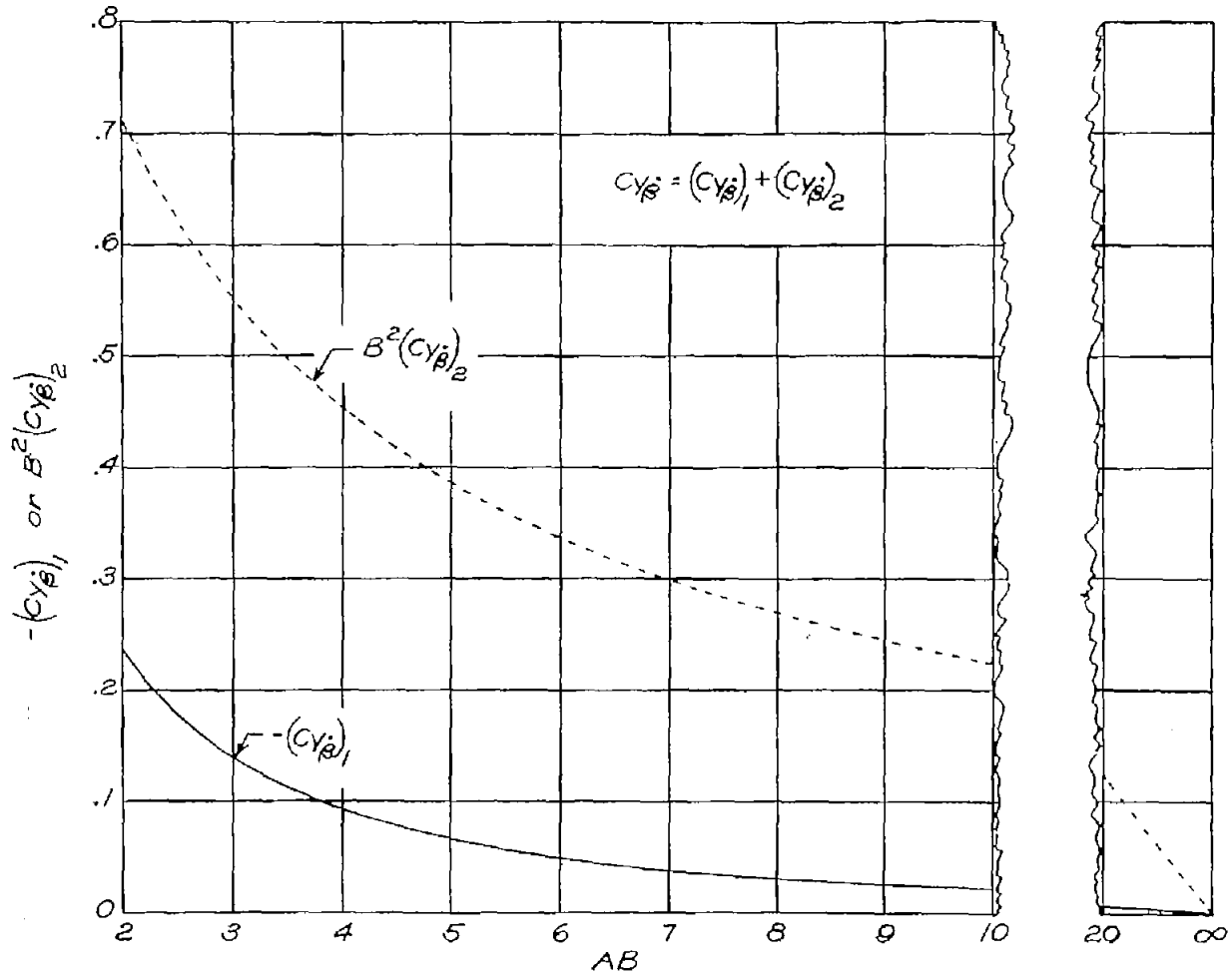

Figure 6.- Curves for determining the stability derivative due to constant lateral acceleration $C_{Y_{\dot{\beta}}}$ for isolated half-delta vertical tails with supersonic leading edges. Derivative based on vertical-tail parameters b, S, and angle $\dot{\beta}b/V$; principal body-axes system.

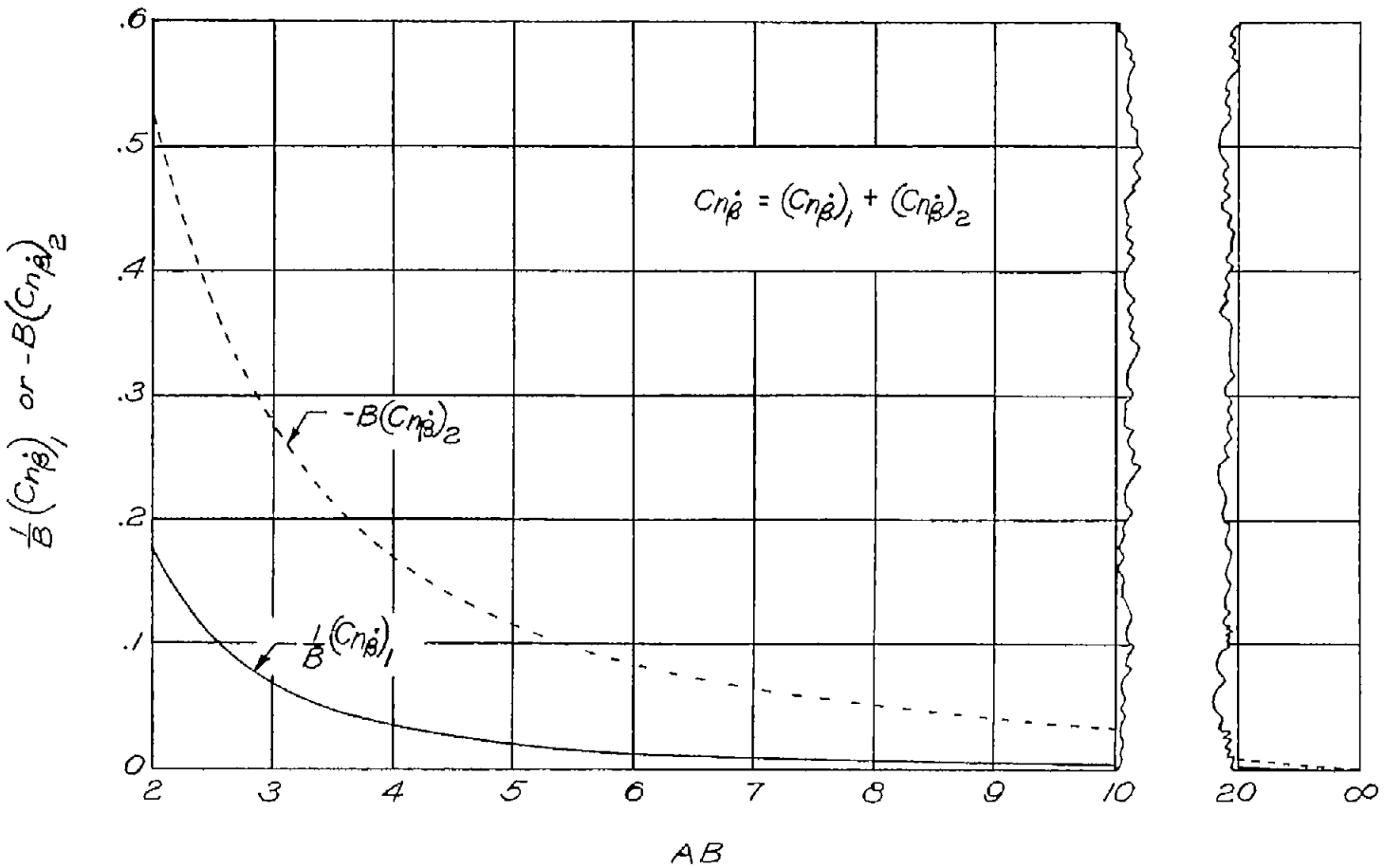

Figure 7.- Curves for determining the stability derivative due to constant lateral acceleration $C_{n_{\dot{\beta}}}$ for isolated half-delta vertical tails with supersonic leading edges. Derivative based on vertical-tail parameters b, S, and angle $\dot{\beta}b/V$; principal body-axes system with origin at leading edge of root section.

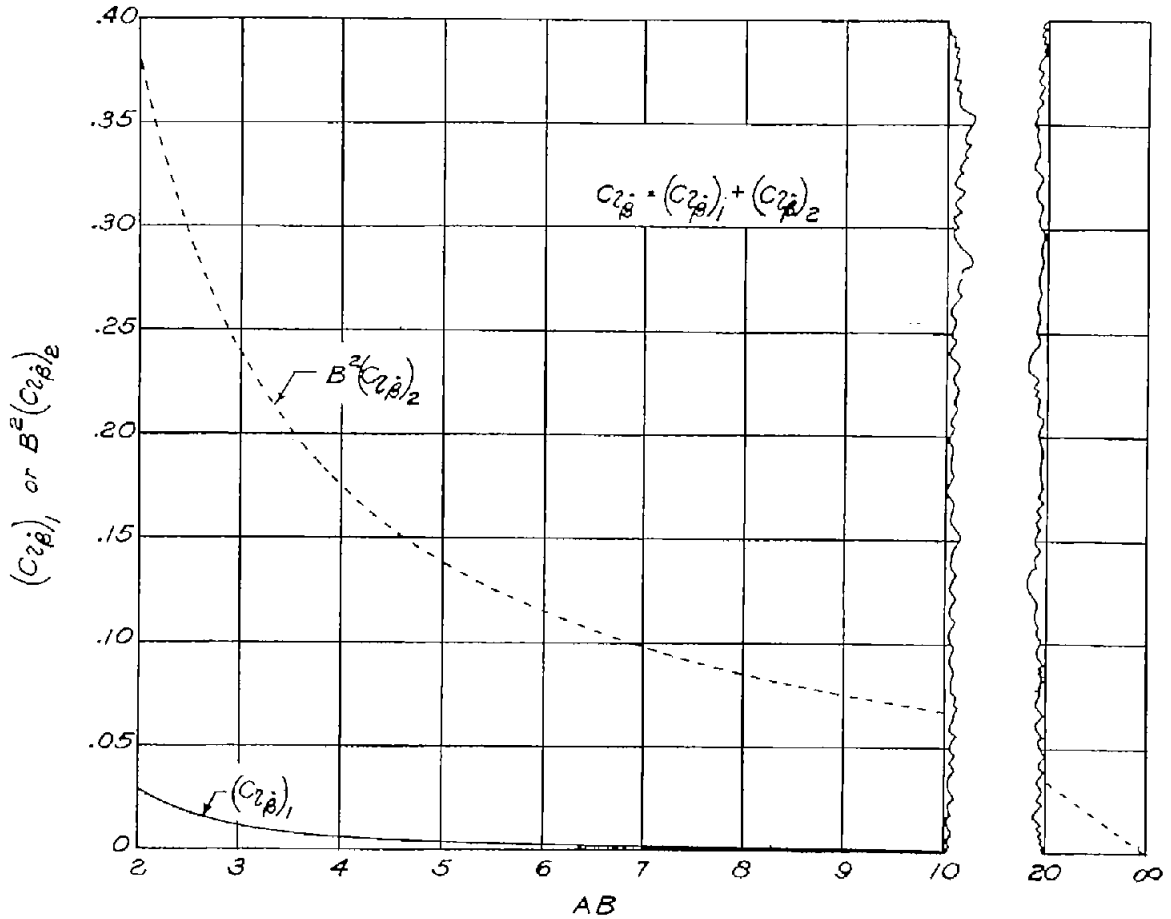

Figure 8.- Curves for determining the stability derivative due to constant lateral acceleration $C_{l_{\dot{\beta}}}$ for isolated half-delta vertical tails with supersonic leading edges. Derivative based on vertical-tail parameters b, S, and angle $\dot{\beta}b/V$; principal body-axes system with origin at leading edge of root section.

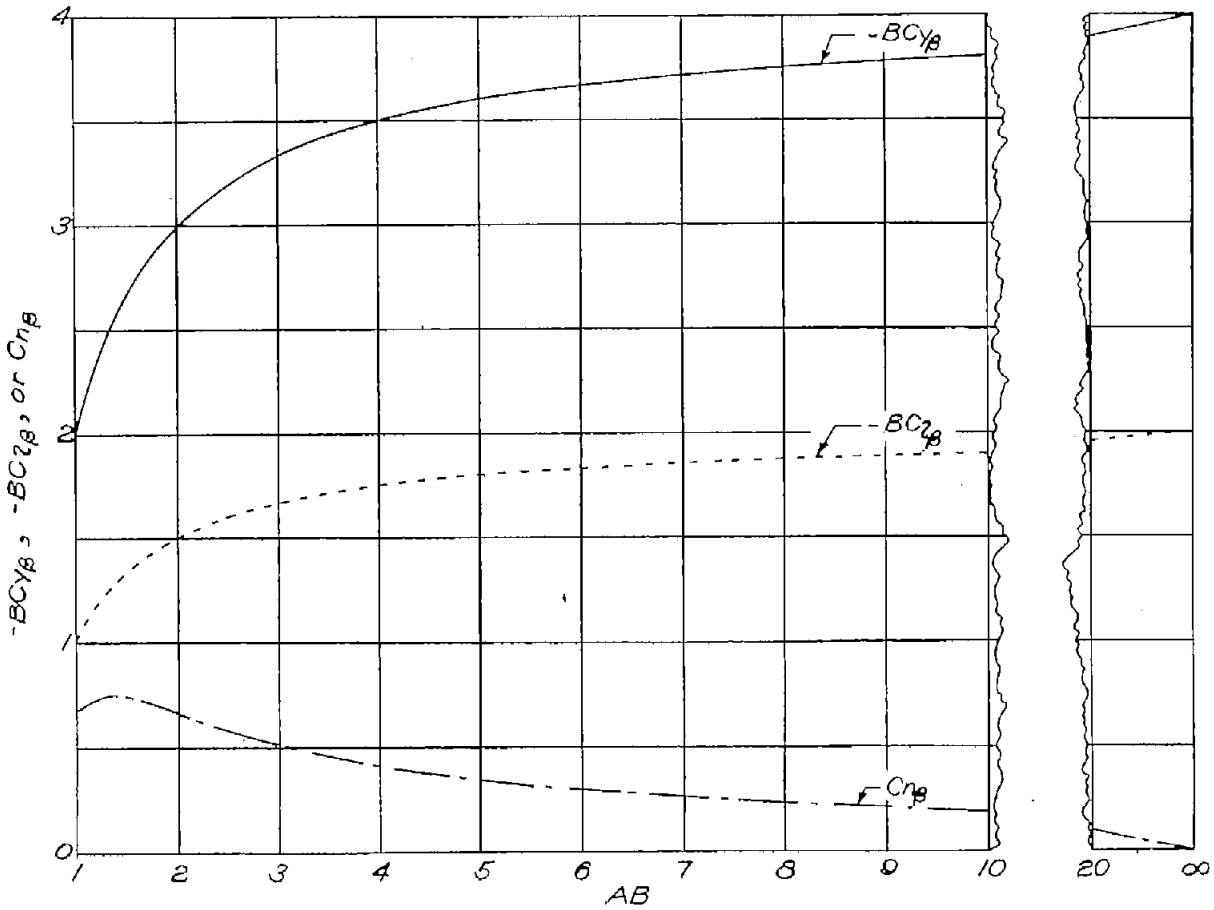

Figure 9.- Curves for determining the stability derivatives due to constant sideslip C_{Y_β}, C_{n_β}, and C_{l_β} for isolated rectangular vertical tails. Derivatives based on vertical-tail parameters b and S; principal body-axes system with origin at leading edge of root section.

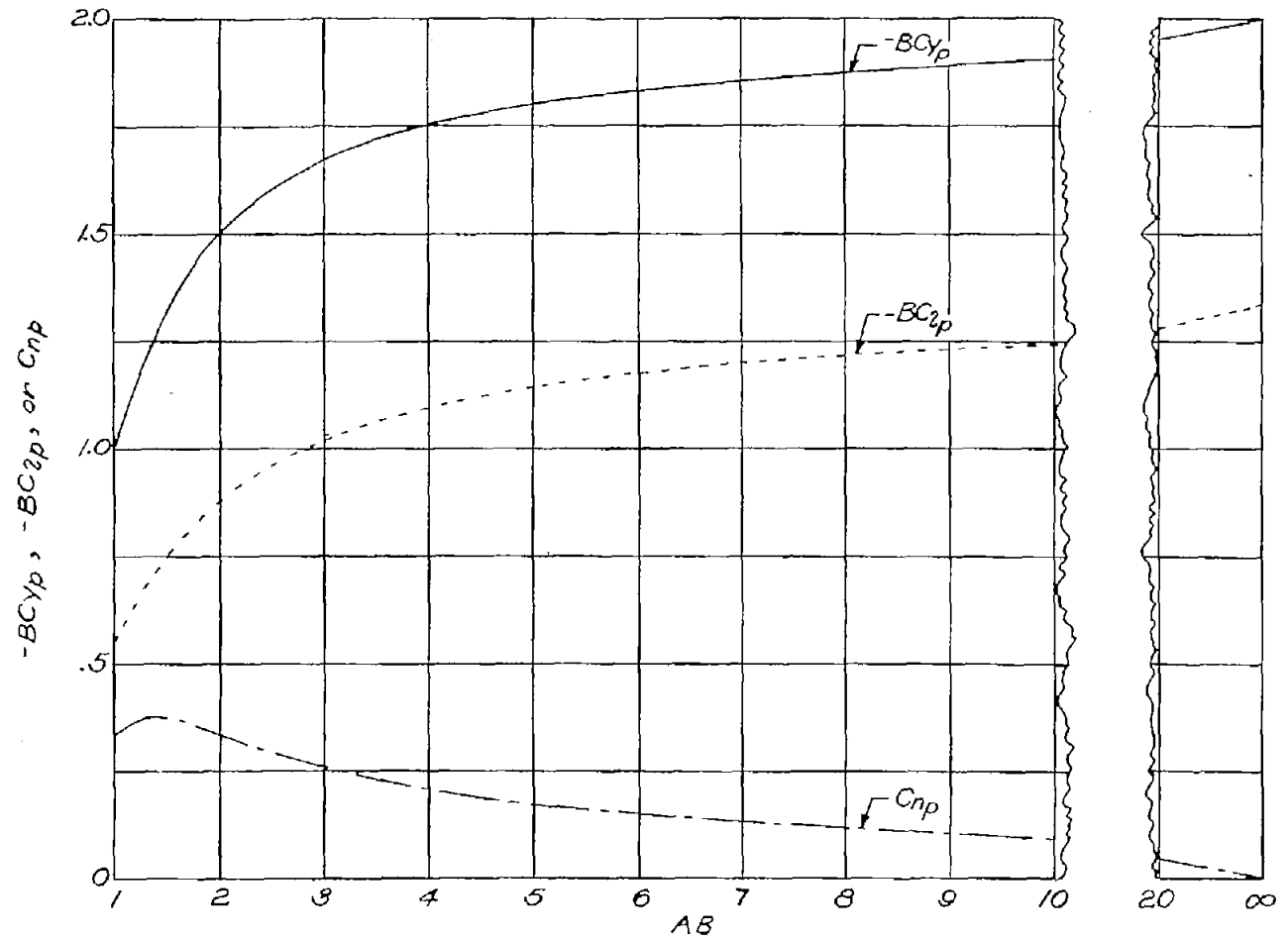

Figure 10.- Curves for determining the stability derivatives due to steady rolling C_{Y_p}, C_{n_p}, and C_{l_p} for isolated rectangular vertical tails. Derivatives based on vertical-tail parameters b, S, and angle pb/V; principal body-axes system with origin at leading edge of root section.

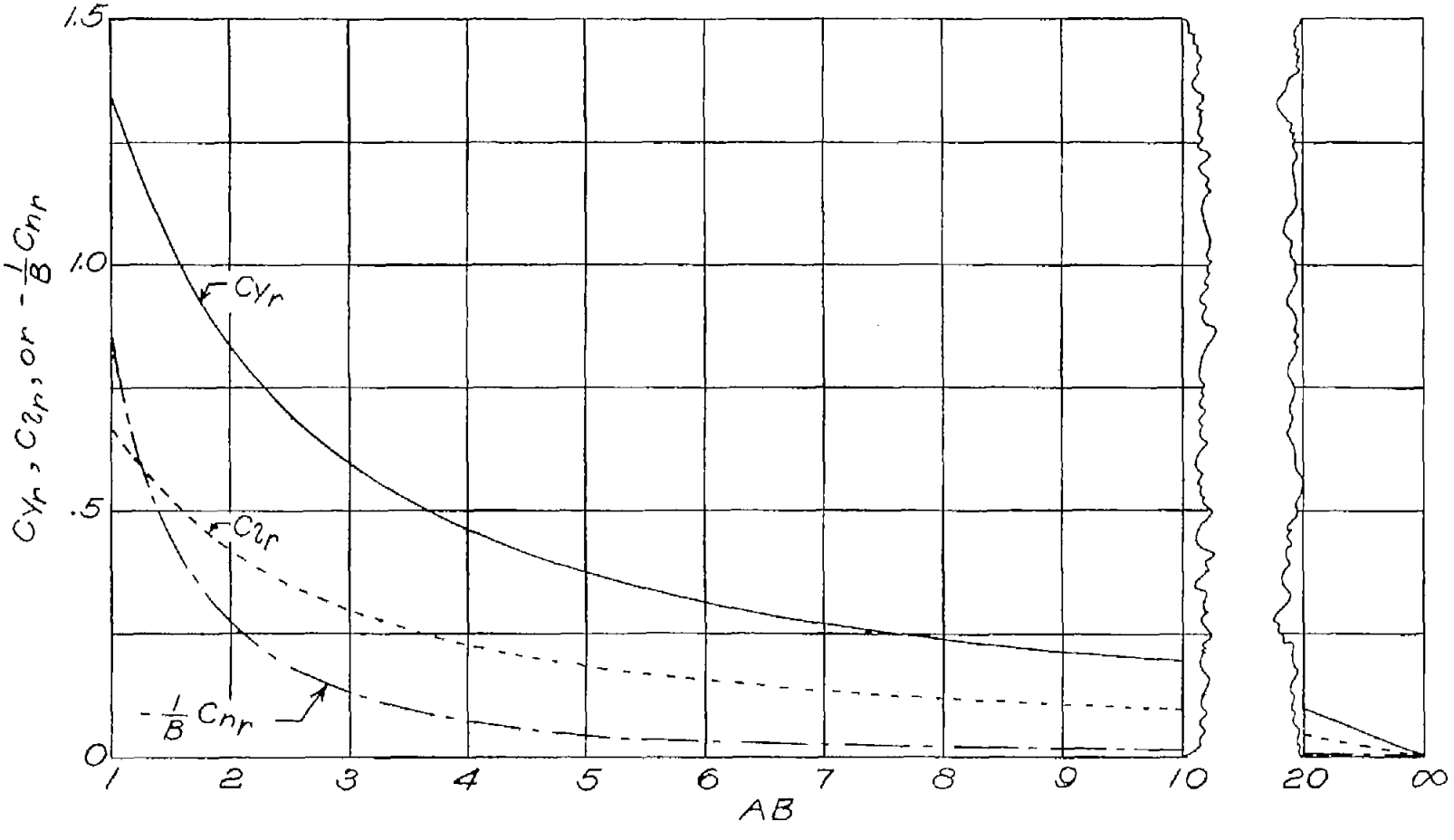

Figure 11.- Curves for determining the stability derivatives due to steady yawing C_{Y_r}, C_{n_r}, and C_{l_r} for isolated rectangular vertical tails.

Derivatives based on vertical-tail parameters b, S, and angle rb/V; principal body-axes system with origin at leading edge of root section.

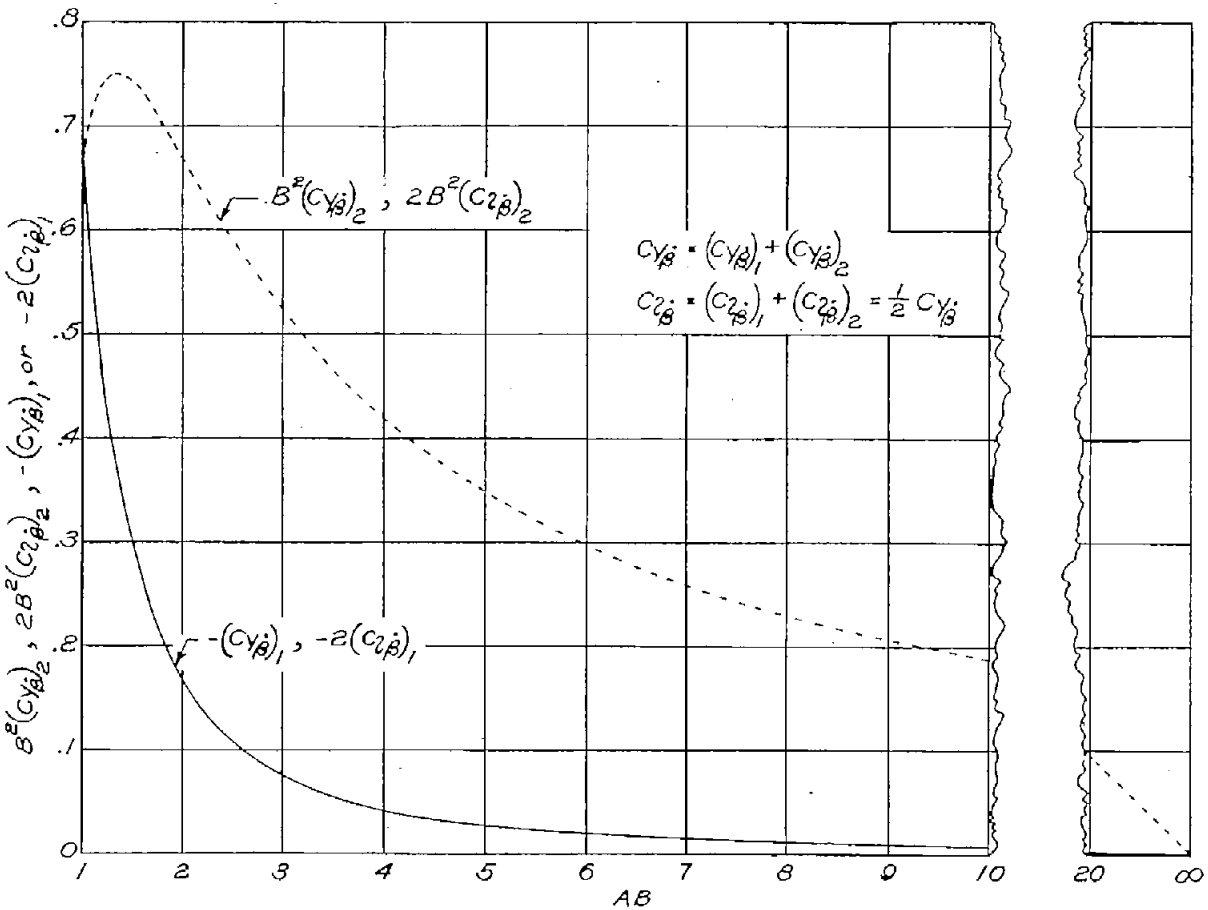

Figure 12.- Curves for determining the stability derivatives due to constant lateral acceleration $C_{Y_{\dot\beta}}$ and $C_{l_{\dot\beta}}$ for isolated rectangular vertical tails. Derivatives based on vertical-tail parameters b, S, and angle $\dot\beta b/V$; principal body-axes system with origin at leading edge of root section.

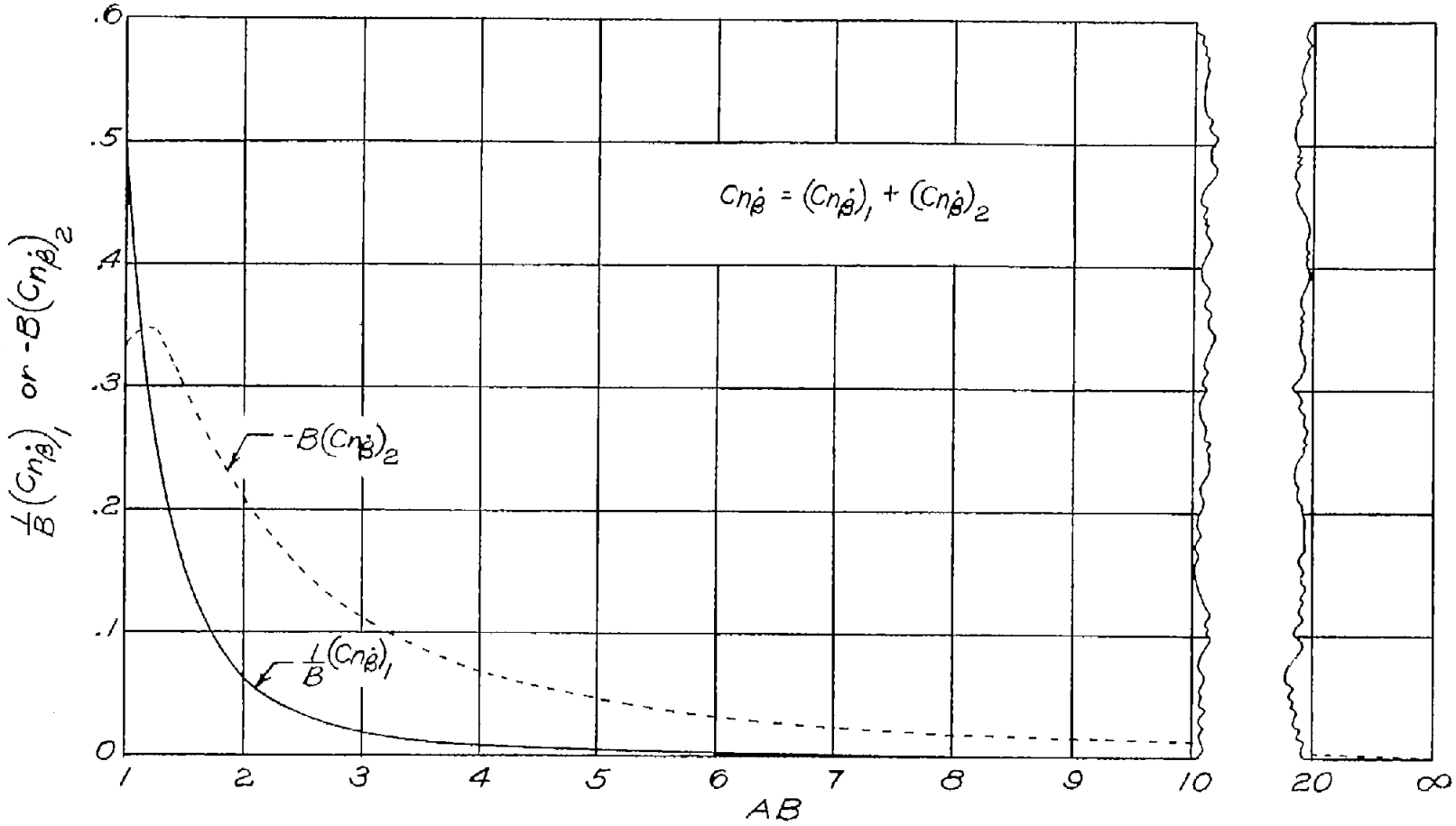

Figure 13.- Curves for determining the stability derivative due to constant lateral acceleration $C_{n_{\dot{\beta}}}$ for isolated rectangular vertical tails. Derivative based on vertical-tail parameters b, S, and angle $\dot{\beta}b/V$; principal body-axes system with origin at leading edge of root section.

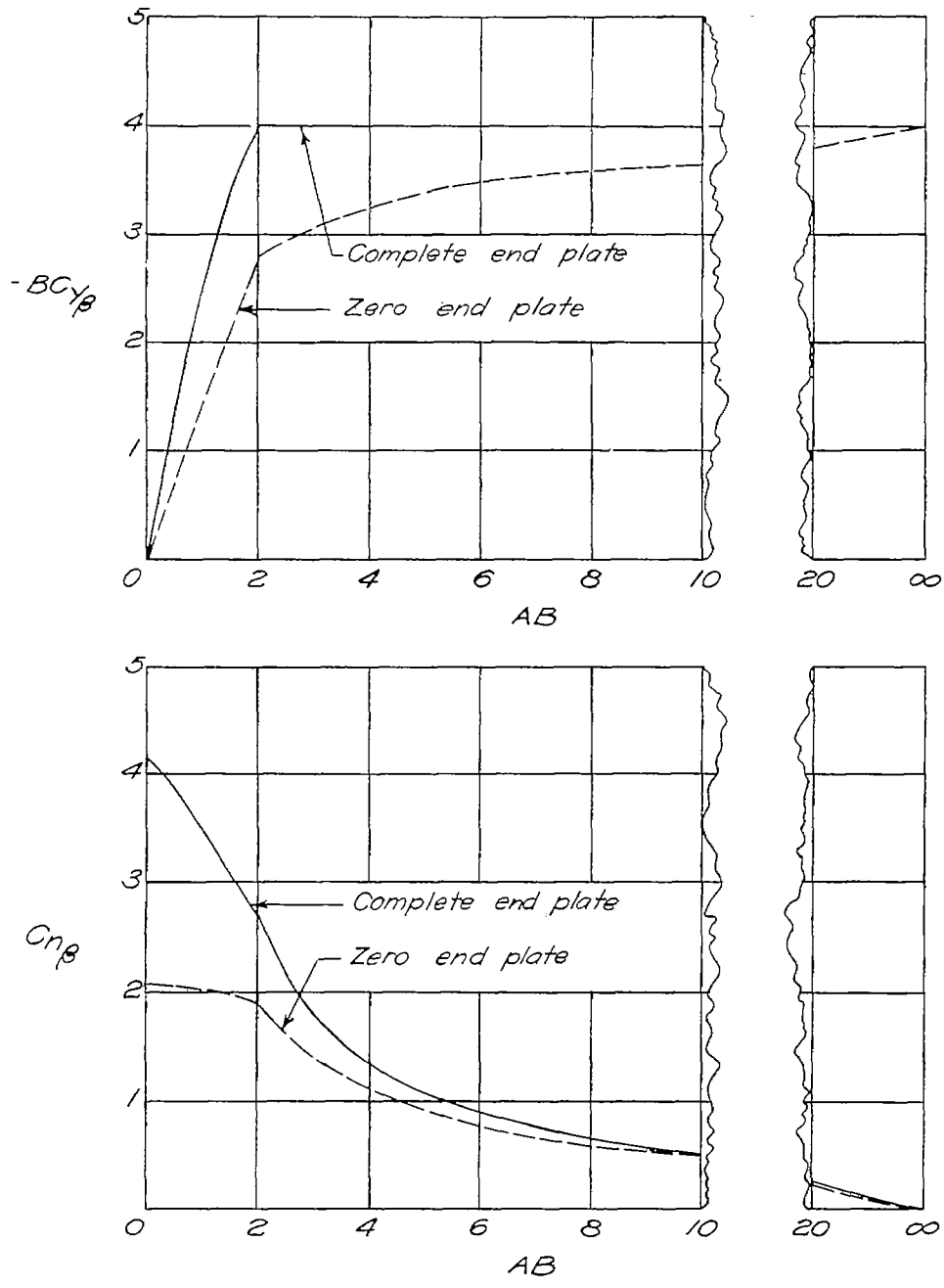

(a) Constant sideslip.

Figure 14.- Comparisons of zero- and complete-end-plate solutions for the side-force and yawing-moment derivatives due to several lateral motions for half-delta vertical tails. Derivatives based on vertical-tail parameters b, S, and angles pb/V, rb/V, and $\dot{\beta}$b/V; principal body-axes system with origin at leading edge of root section.

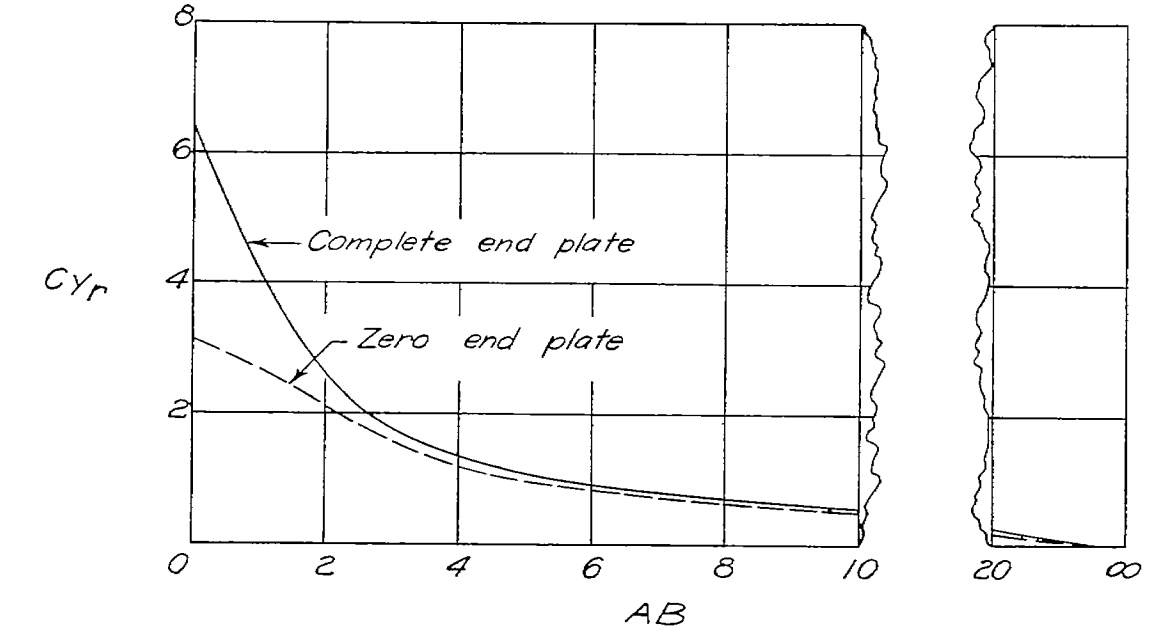

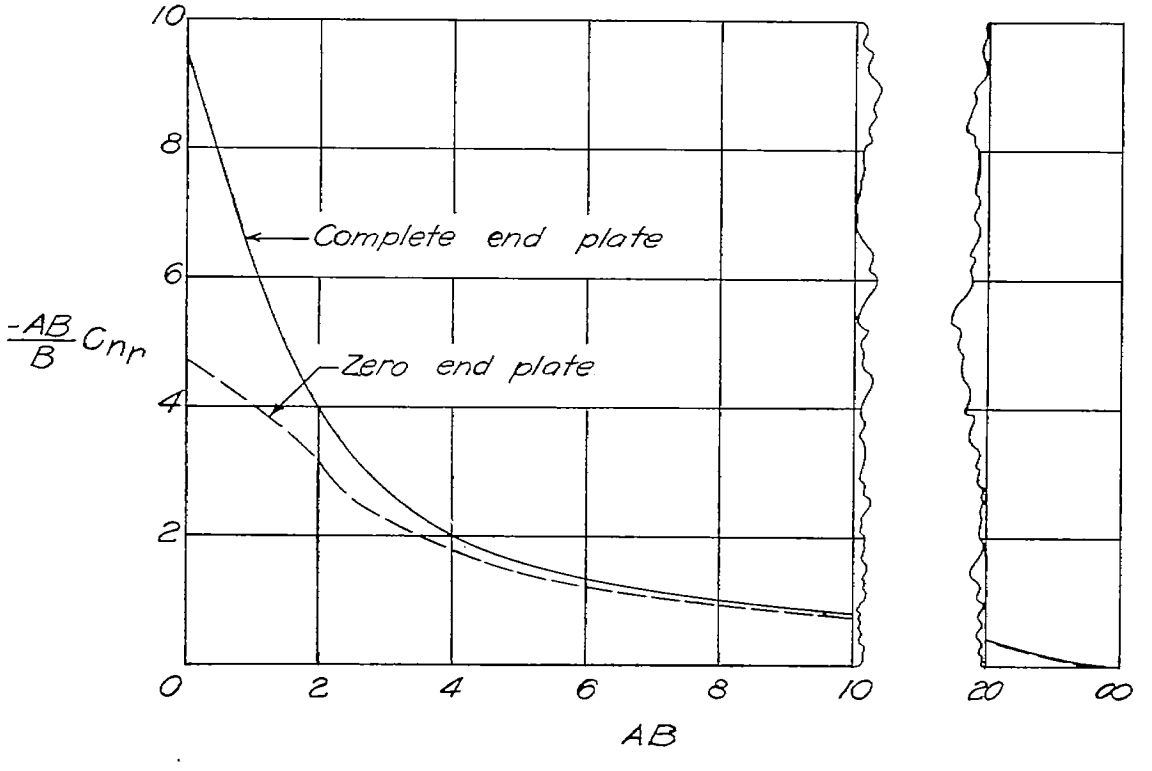

(b) Steady yawing.

Figure 14.- Continued.

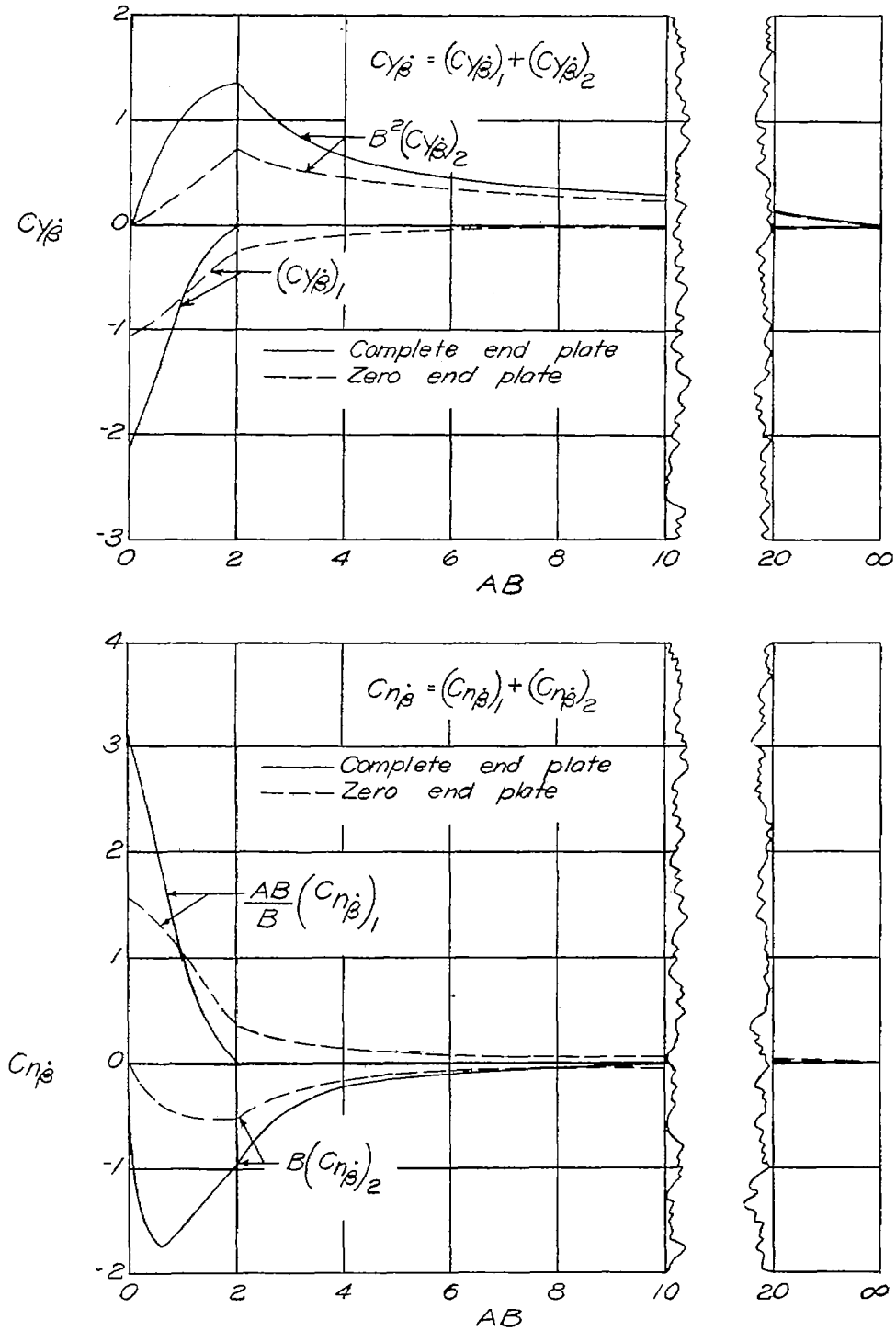

(c) Constant lateral acceleration.

Figure 14.- Concluded.

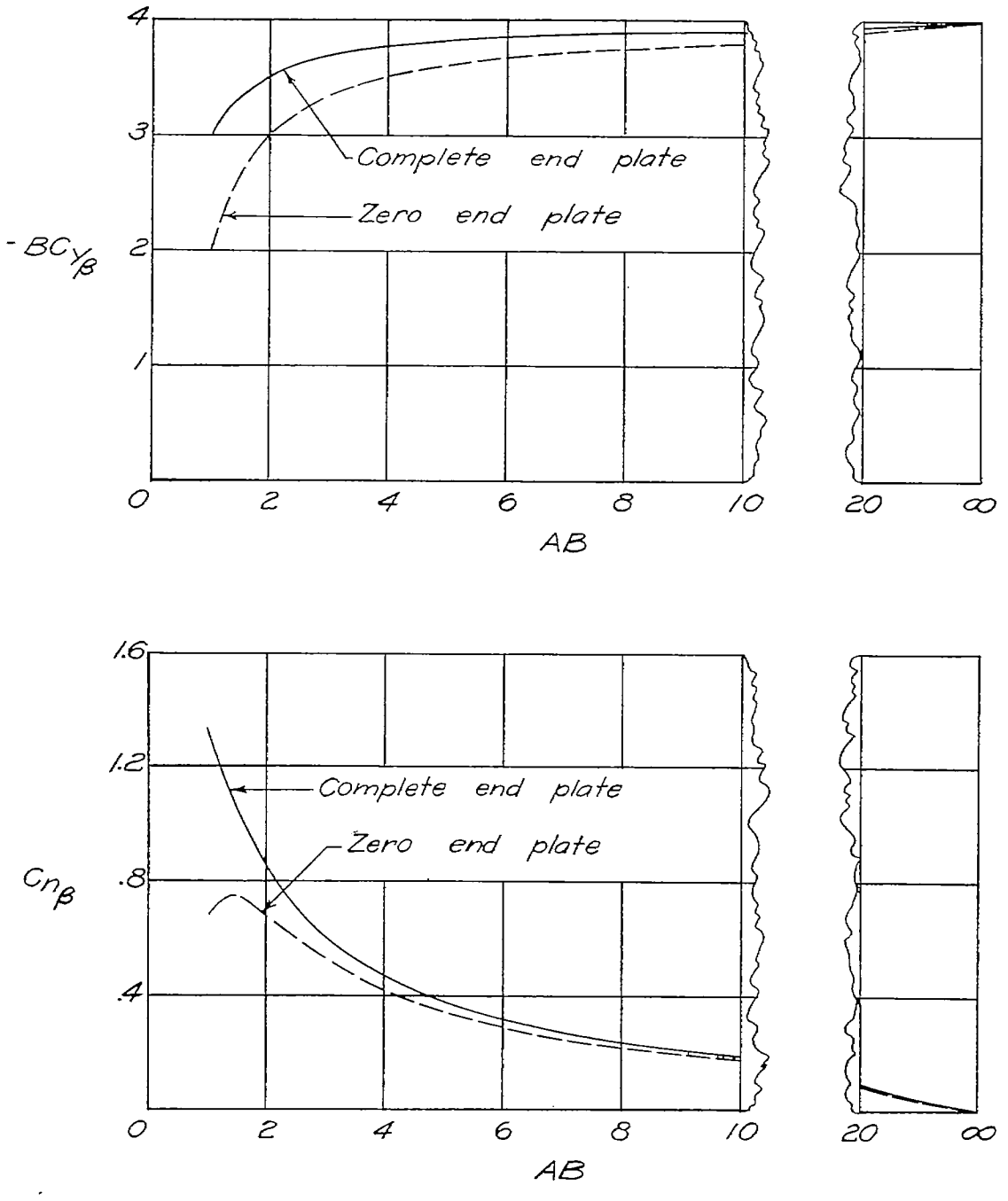

(a) Constant sideslip.

Figure 15.- Comparisons of zero- and complete-end-plate solutions for the side-force and yawing-moment derivatives due to several lateral motions for rectangular vertical tails. Derivatives based on vertical-tail parameters b, S, and angles pb/V, rb/V, and $\dot{\beta}$b/V; principal body-axes system with origin at leading edge of root section.

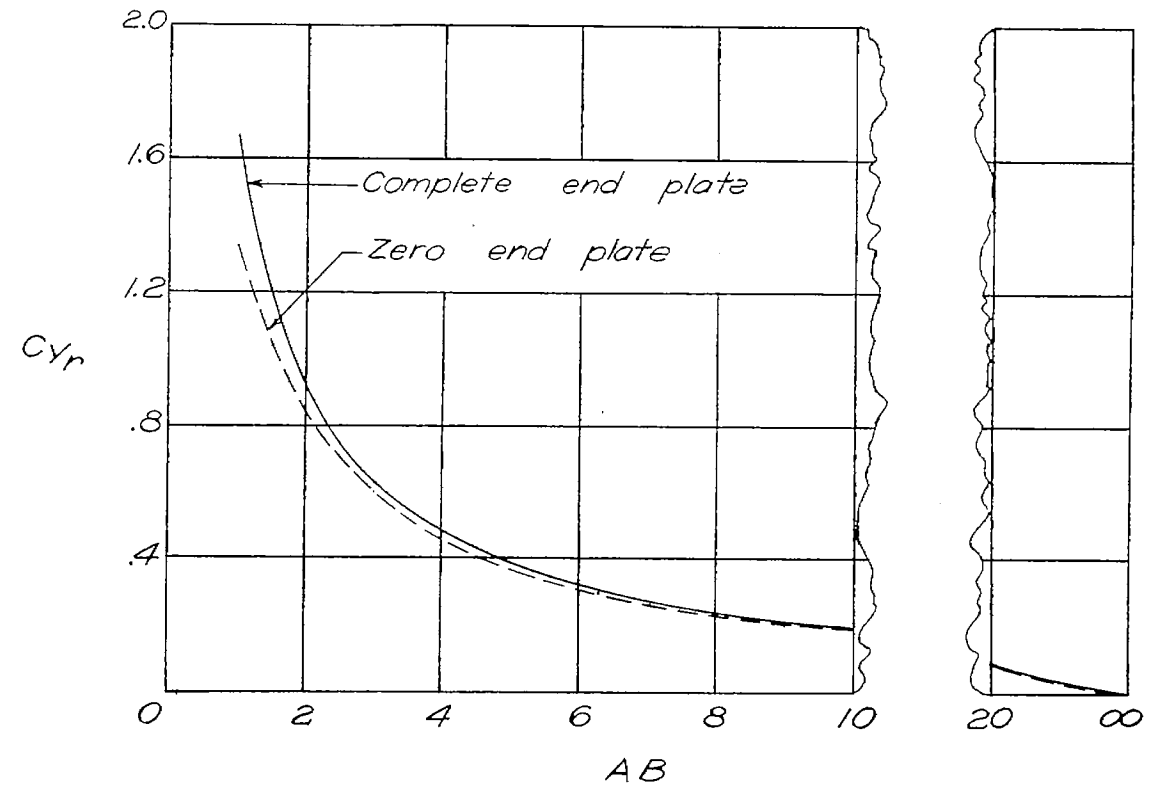

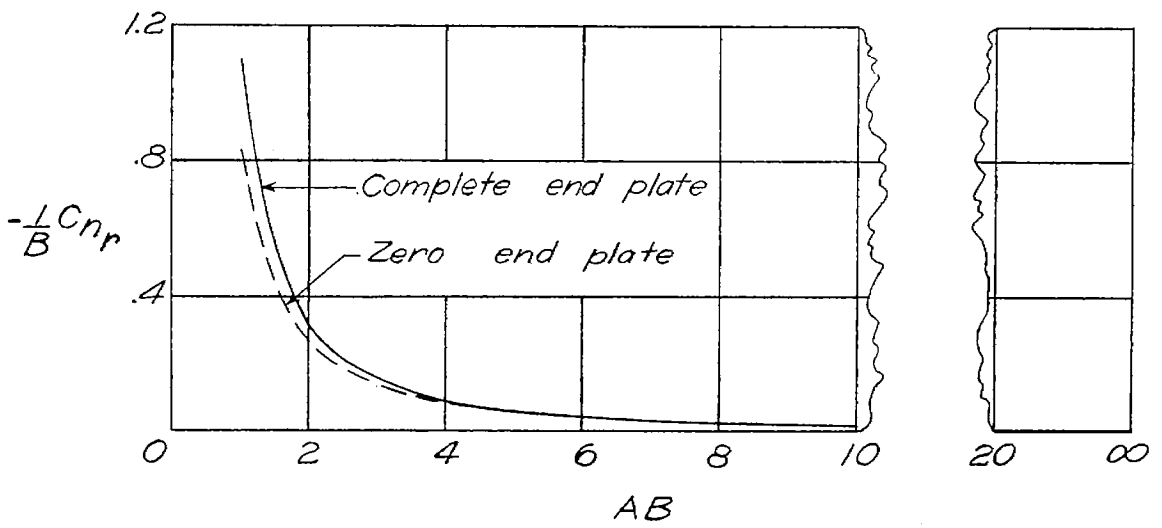

(b) Steady yawing.

Figure 15.- Continued.

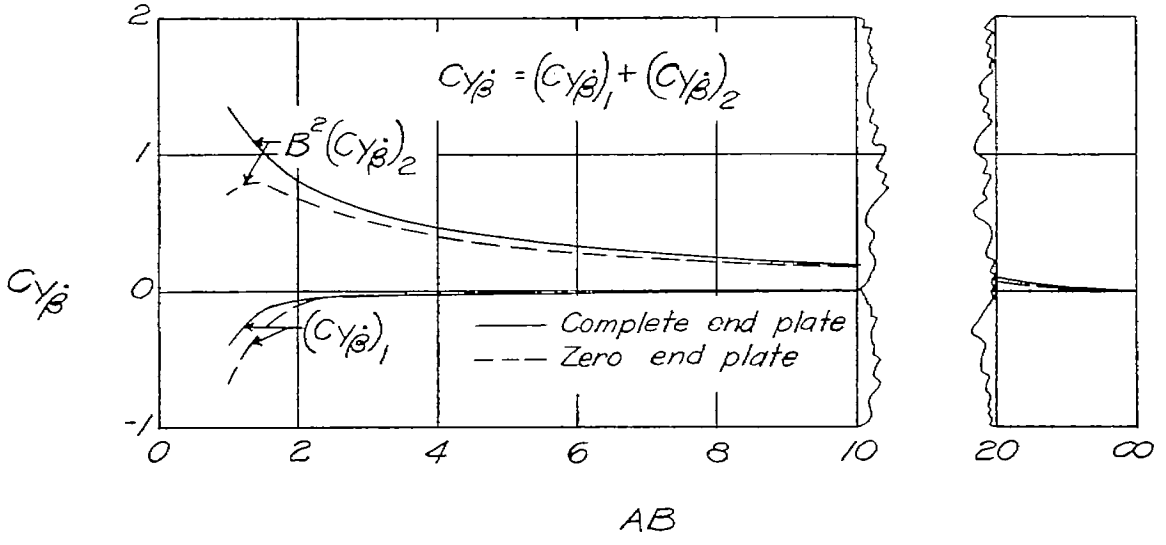

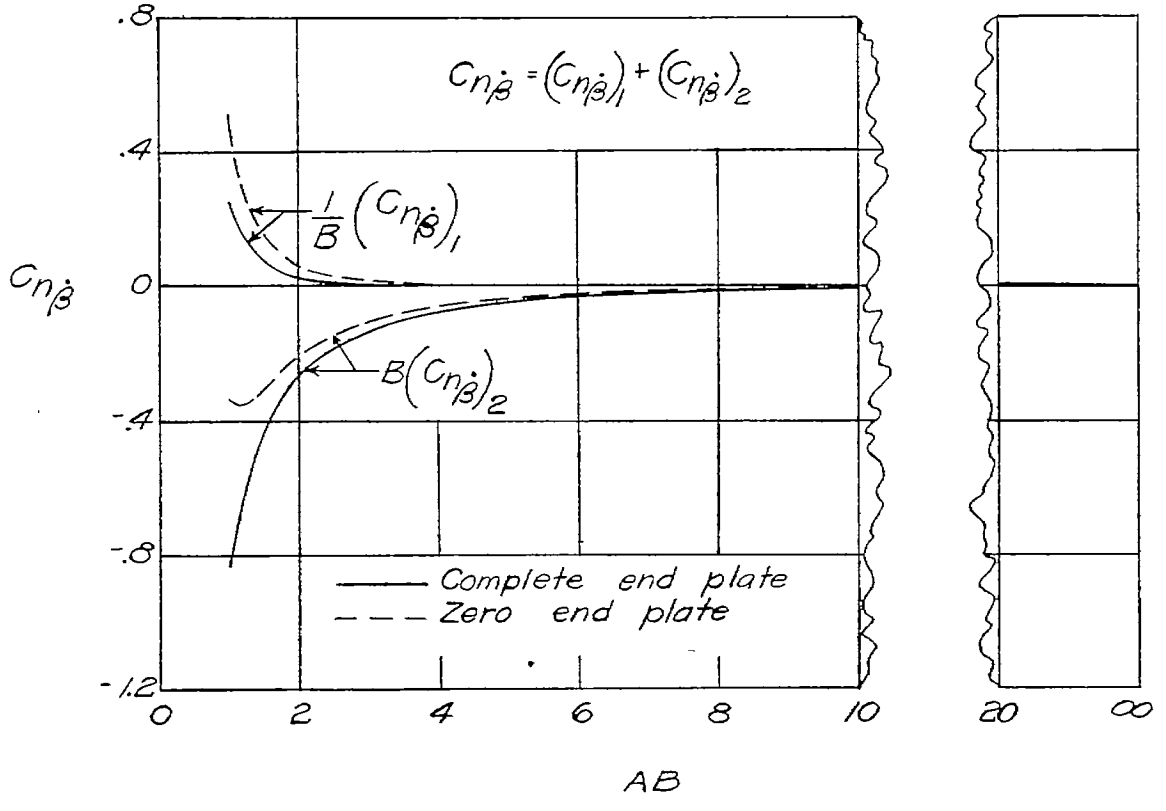

(c) Constant lateral acceleration.

Figure 15.- Concluded.

NACA-Langley - 3-29-55 - 1000